

Thermal effect on magnetoexciton energy spectra in monolayer transition-metal dichalcogenides

Duy-Nhat Ly,^{1,*} Dai-Nam Le,^{2,†} Ngoc-Hung Phan,¹ and Van-Hoang Le^{1,‡}

¹Computational Physics Key Laboratory K002, Department of Physics,
Ho Chi Minh City University of Education, Ho Chi Minh City 72759, Vietnam[§]

²Department of Physics, University of South Florida, Tampa, FL 33620, United States of America[§]
(Dated: April 07, 2023)

It is widely comprehended that temperature may cause phonon-exciton scattering, enhancing the energy level's linewidth and leading to some spectrum shifts. However, in the present paper, we suggest a different mechanism that allows the thermal motion of the exciton's center of mass (c.m.) to affect the magnetoexciton energies in monolayer dichalcogenides (TMDCs). By the nontrivial but precise separation of the c.m. motion from an exciton in a monolayer TMDC with a magnetic field, we obtain an equation for the relative motion containing a motional Stark term proportional to the c.m. pseudomomentum, related to the temperature of the exciton gas but neglected in the previous studies. Solving the Schrödinger equation without omitting the motional Stark potential at room temperature shows approximately a few meV thermal-magnetic shifts in the exciton energies, significant enough for experimental detection. Moreover, this thermal effect causes a change in exciton radius and diamagnetic coefficient and enhances the exciton lifetime as a consequence. Surprisingly, the thermoinduced motional Stark potential breaks the system's SO(2) symmetry, conducting new peaks in the exciton absorption spectra at room temperature besides those of the s states. This mechanism could be extended for other magnetoquasiparticles such as trions and biexcitons.

Preprint of *Phys. Rev. B* **107**, 155410 (2023) [1].

Keywords: exciton, transition-metal dichalcogenides, finite temperature, motional Stark potential, thermal effect

I. INTRODUCTION

During the last two decades, monolayer transition-metal dichalcogenides (TMDCs) have become hot spots for papering the formation of excitons because of their unique property of electron-hole interaction [2–5]. Unlike three-dimensional excitons in novel semiconductors, neutral excitons in these monolayer TMDCs are thermally stable at room temperature, even for the Rydberg states. Their high binding energy provides beneficial optical properties in both ultraviolet (UV) and infrared (IR) ranges [6–10]. Especially, exciton energy spectra under the presence of a constant magnetic field have been of great interest recently both in experimental observations and theoretical studies due to their incredible potential in retrieving several physical quantities of monolayer TMDCs, such as effective masses of electrons and holes, the Landé g factors, and two-dimensional polarizability [11–23]. Therefore, it is essential to qualitatively (and quantitatively, if possible) comprehend the influences of external factors like temperature on the energy spectra of magnetoexcitons in the monolayer TMDCs.

The thermal effect on the exciton energies has been intensively investigated recently and explained by the

exciton-phonon scattering [24, 25]. Indeed, the quantization of the crystal lattice oscillation results in quasiparticles named *phonons* which carry the thermal motion. The scattering between excitons and phonons affects the relative motion of the electron-hole pair that, consequently, causes some energy shifts of the exciton bound states. Recently, experiments for exciton energies in monolayer TMDCs have been conducted with a high magnetic field [20–22], raising another question related to the center of mass (c.m.) separation. It is well known that the c.m. of a two-body system in a magnetic field can be separated, but the c.m. pseudomomentum remains in the equation for relative motion [26–28]. This circumstance leads to a mechanism that the thermal motion of the c.m. can affect the exciton energies. We will

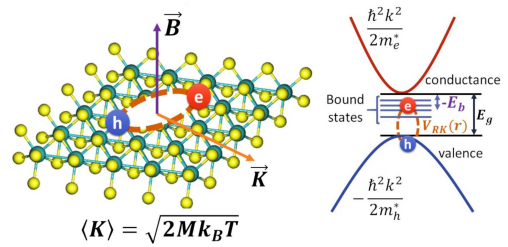


FIG. 1. (Color online) Excitons in a monolayer TMDC with a magnetic field. The c.m. pseudomomentum is conserved and related to the thermal motion.

* nhatld@hcmue.edu.vn

† dainamle@usf.edu

‡ hoanglv@hcmue.edu.vn

§ These authors contributed equally to this paper.

show in the present paper additional energy shifts caused by this thermal-magnetic effect.

The exciton-phonon scattering at finite temperatures affects the imaginary part of exciton energy that makes exciton decay [4, 29–35]. However, in our thermal-magnetic mechanism, the motional Stark potential, linearly proportional to the magnetic intensity, could be more inconspicuous than the diamagnetic potential depending on the squared magnetic intensity and may contribute only to the energy shift but not to the exciton lifetime. Nevertheless, this thermoinduced potential could make the average radius of the electron-hole pair larger and consequently enhance the radiative lifetime of excitons in monolayer TMDCs [30, 34, 35]. Besides, the symmetry breaking of the system due to the additional thermoinduced term can affect the wave functions. Therefore, we aim to examine the effect of finite temperature on the exciton energy spectra, the diamagnetic coefficient, and the exciton radius as a function of magnetic intensity and their consequence on the absorption spectra and the exciton radiative lifetime.

The rest of this paper is as follows. Section II presents the theoretical background for our paper, including the separation of the c.m. motion, the introduction of the motional Stark potential, and the assumption about its temperature dependence. Then, the results and discussion are given in Sec. III with the thermal effect on the diamagnetic coefficients, the thermal-magnetic shift on exciton energies, the thermoinduced symmetry-breaking and enhancement of exciton lifetime, and the new peaks in absorption spectra. Section IV includes our conclusion.

II. THEORETICAL BACKGROUND

A. Schrödinger equation

To consider the thermal effect, we need to solve the Schrödinger equation of the electron-hole pair in the framepaper of the effective mass approximation, where a Wannier exciton in a monolayer TMDC is described as a two-dimensional system of one electron and one hole interacting with each other by the potential $\hat{V}_{h-e}(r)$ in the xy plane, as shown in Fig. 1. Because of the two-dimensional many-particle effect, the interaction potential \hat{V}_{h-e} is no longer Coulombic but screened and described by the Rytova-Keldysh potential [2, 3, 36–39]. One required task before solving the Schrödinger equation is to separate the movement of the electron-hole c.m. with the coordinate \mathbf{R} . However, for a two-body system such as an exciton in a magnetic field $\mathbf{B} = B\mathbf{e}_z$, the c.m. dynamics can not be removed totally from the equation describing the electron-hole relative motion. The variable-separation procedure for this system is no longer trivial because the magnetic field breaks the system's translation symmetry, which leads to the nonconservation of the total momentum \mathbf{P} of the electron-hole pair.

Fortunately, there is instead another constant of motion, pseudomomentum $\hat{\mathbf{P}}_0 = \hat{\mathbf{P}} - \frac{1}{2}e\mathbf{B} \times \mathbf{r}$, commuting with the system's Hamiltonian, i.e., $[\hat{\mathbf{P}}_0, \hat{H}_X] = 0$. Using this conservative quantity, one can obtain an equation for the relative motion [26–28]. In this case, the wave function can be written as

$$\Psi_{\mathbf{K}}(\mathbf{R}, \mathbf{r}) = e^{\frac{i}{\hbar}(\mathbf{K} + \frac{1}{2}e\mathbf{B} \times \mathbf{r}) \cdot \mathbf{r}} \psi_{\mathbf{K}}(\mathbf{r}), \quad (1)$$

where \mathbf{K} is an eigenvector of operator $\hat{\mathbf{P}}_0$. The wave function for relative motion $\psi_{\mathbf{K}}(\mathbf{r})$ is obtained by solving the Schrödinger equation

$$\left\{ \frac{\hat{\mathbf{p}}^2}{2\mu} + \frac{1-\sigma}{1+\sigma} \frac{eB}{2\mu} \hat{l}_z + \frac{e^2 B^2}{8\mu} r^2 + \hat{V}_{h-e}(r) - \frac{e}{M} (\mathbf{B} \times \mathbf{K}) \cdot \mathbf{r} - E \right\} \psi_{\mathbf{K}}(\mathbf{r}) = 0. \quad (2)$$

with the total mass $M = m_e^* + m_h^*$, the exciton reduced mass $\mu = m_e^* m_h^* / (m_e^* + m_h^*)$, and the ratio of masses $\sigma = m_e^* / m_h^*$. Here, m_e^* and m_h^* are the effective masses of the electron and hole; e is the elementary charge with the positive value; $\hat{\mathbf{p}}$ and \hat{l}_z are the operators of the momentum and angular momentum of the relative motion. A detailed derivation of Eq. (2) is given in Suppl. [40].

For the exciton in monolayer TMDCs such as WSe₂ as considered in this paper, the exciton reduced mass $\mu = 0.20 \times m_e$, mass ratio $\sigma = 0.94$, total mass $M = 0.80 \times m_e$ (m_e is electron mass), and the Rytova-Keldysh potential's parameters (the average dielectric constant of the surrounding material $\kappa = 4.5$, screening length $r_0 = 4.21$) are taken from Refs. [16, 21].

B. Thermoinduced motional Stark potential

In equation (2), we consider the specific term $V_{mS} = -\frac{e}{M} (\mathbf{B} \times \mathbf{K}) \cdot \mathbf{r}$ containing the c.m. pseudomomentum \mathbf{K} and will show its relation to the temperature of the neutral exciton gas. First, we note that the density of excitons n_X in monolayer TMDCs is low, i.e., the average distance between two excitons $1/\sqrt{n_X}$ is much larger than the thermal wavelength $\lambda_{th} = \sqrt{\frac{2\pi\hbar^2}{Mk_B T}}$ so that the Maxwell-Boltzmann statistics is still valid. Indeed, the density n_X , i.e., the number of neutral excitons per unit of area, could be modulated around 10^{11} – 10^{12} cm⁻² in real experiments for monolayer WSe₂ [41–44], which is much smaller than its limit at room temperature $\lambda_{th}^{-2} = 4.3 \times 10^{12}$ cm⁻². Then, we estimate the root-mean-square of the c.m. pseudomomentum at temperature T by the equipartition theorem as $\frac{1}{2M} \overline{K^2} = k_B T$, where k_B is the Boltzmann constant. Instead of calculating exciton energies at each pseudomomentum value and then averaging them as $\overline{E(K)}$, we do it another way by calculating the exciton energy $E(\overline{K})$ at the average pseudomomentum value. The validity of this approach has been confirmed numerically in Tab.S-I in Suppl. [40]. This approach allows the considered potential to relate to the temperature

as follows

$$V_{mS}(\mathbf{r}) = -\sqrt{\frac{2k_B T}{M}} eBx. \quad (3)$$

Here, without losing generality, we consider the case where \mathbf{K} is along the y axis so that vector $\mathbf{B} \times \mathbf{K}$ is along the x axis. A more microscopic grounding for the thermoinduced term (3) is given in Sec.S-V and Sec.S-VI in Suppl. [40].

The potential (3) influences the exciton in the same way as the Stark effect [45, 46], so we call it *thermoinduced motional Stark potential*. Recent theoretical studies of magnetoexcitons in monolayer TMDCs always neglect this potential [15, 19, 22] that is reasonable only at zero temperature. However, the experimental observations were conducted not only at low temperatures [12, 14, 16–18, 20, 21] but also at room temperature [10, 11, 24, 25]. Hence, the motional Stark effect arising from the thermal fluctuation of the c.m. pseudomomentum needs to be considered when calculating the energy spectra of magnetoexcitons in monolayer TMDCs.

We can see that the diamagnetic term $V_{diamag.}(\mathbf{r}) = \frac{e^2 B^2}{8\mu} r^2$ in the effective potential of Eq. (2) is quadratically proportional to the electron-hole distance and consequently dominant at the large separation of the electro-hole pair compared to the thermoinduced Stark term, which is linearly proportional to the variable x . As a result, there is no tunneling effect, even considering the thermoinduced motional Stark potential. The exciton is always in its bound states, unlike the well-known LoSurdo-Stark effect in the two-dimensional electron gas [47, 48] and field-induced dissociation of excitons in a TMDC [49]. Instead of tunneling, we expect the thermoinduced motional Stark potential could cause the Stark shift in the energy spectra.

III. RESULTS AND DISCUSSION

A. Thermal effect on diamagnetic coefficient and Landau levels

To see how the thermoinduced motional Stark potential affects the asymptotic behaviors of exciton energies in the limits of low and high magnetic intensities, we calculate the energies analytically by applying the perturbation theory to the Schrödinger equation (2). For low magnetic intensity, restricted by the condition that the typical length in the magnetic field is much larger than the average exciton radius: $l_B = \sqrt{\hbar/eB} \gg \langle r \rangle_{nm}$, we have the energy of the (n, m) quantum state in the second perturbation order as

$$E_{nm}^{(2)}(B, T) = E_{nm}^{(0)} + \frac{1 - \sigma}{1 + \sigma} \frac{m\hbar}{2\mu} eB + \frac{\langle r^2 \rangle_{nm}}{8\mu} e^2 B^2 - \alpha_{nm} \frac{k_B T}{M} e^2 B^2, \quad (4)$$

where $E_{nm}^{(0)}$, $\langle r^2 \rangle_{nm}$, and α_{nm} are the zero-field energy, squared radius, and polarizability of the exciton. To calculate these quantities, we need to solve the Schrödinger equation in the zeroth order of approximation. However, the solutions cannot be obtained analytically, so, we do it another way by numerically solving equation (2) and then fitting the obtained results to formula (4). The concrete values are presented in Table I for $1s$, $2s$, $3s$, $2p_{-1}$, and $2p_{+1}$ states.

TABLE I. Zero-field energies, squared radius, and polarizability.

	$1s$	$2s$	$3s$	$2p_{-1}$	$2p_{+1}$
$E_{nm}^{(0)}$ (eV)	-0.1686	-0.0386	-0.0166	-0.0498	-0.0498
$\langle r^2 \rangle_{nm}$ (nm ²)	2.63	45.8	241	21.1	21.1
α_{nm} (nm ² /eV)	3.91	-112	-6060	259	240

The last term in the exciton energy (4), the motional Stark correction, is quadratically proportional to the magnetic field (see also in Fig.S-2 in Suppl. [40]). That means the thermal effect contributes to the diamagnetic coefficient σ_{nm} defined by the equation

$$\begin{aligned} \sigma_{nm}(T) &= \lim_{B \rightarrow 0} \frac{1}{2} \frac{\partial^2 E_{nm}(B, T)}{\partial B^2} \\ &= \frac{e^2}{8\mu} \langle r^2 \rangle_{nm} - \frac{e^2}{M} \alpha_{nm} k_B T. \end{aligned} \quad (5)$$

Table II shows some values for the zero-temperature diamagnetic coefficient $\sigma_{nm}^0 = \frac{e^2}{8\mu} \langle r^2 \rangle_{nm}$ and their thermoinduced corrections $\Delta\sigma_{nm} = -\frac{e^2}{M} \alpha_{nm} k_B T$ for the $1s$, $2s$, $3s$, $2p_{-1}$, and $2p_{+1}$ states at room temperature. The thermoinduced corrections are about 8% for $1s$, 13% for $2s$, and extremely high for higher states: $2p_{+1}$, $2p_{-1}$, and $3s$ (56%, 60%, and 130%). These are significant enough to impact experimental measurement that we should pay attention to them when measuring exciton energies at finite temperatures.

TABLE II. Zero-temperature diamagnetic coefficients and their thermoinduced corrections at room temperature in unit of $\mu\text{eV}/\text{Tesla}^2$ compared to the experimental data [16].

	$1s$	$2s$	$3s$	$2p_{-1}$	$2p_{+1}$
σ_{nm} [16]	0.31 ± 0.02	4.6 ± 0.2	22 ± 2	-	-
σ_{nm}^0	0.289	5.039	26.53	2.429	2.429
$\Delta\sigma_{nm}$	-0.022	0.637	34.42	-1.469	-1.361
$\frac{ \Delta\sigma_{nm} }{\sigma_{nm}^0}$	8%	13%	130%	60%	56%

For high magnetic intensity, restricted by condition $l_B = \sqrt{\hbar/eB} \ll \langle r \rangle_{nm}$, the harmonic oscillator potential becomes dominant compared to the Rytova-Keldysk potential. In this case, the main part of the Hamiltonian is the magnetic term; therefore, we can obtain the Landau levels for energies with the thermoinduced Stark

corrections by the perturbation theory as

$$E_{nm}^{(2)}(B, T) = \frac{\hbar}{2\mu} \left(2n - |m| - 1 + \frac{1 - \sigma}{1 + \sigma} m \right) eB - \frac{8\mu\beta_{nm}}{M} k_B T, \quad (6)$$

where the dimensionless coefficients β_{nm} are independent of the temperature T , see details in Suppl. [40]. Because of the neglect of Coulomb interaction, the energy formula (6) is valid only for very high magnetic intensity, extremely higher than the laboratory limit of about 91 Tesla [21]. Nevertheless, this formula gives the right rule for thermoinduced shifts from the Landau levels $\Delta E = -\frac{8\mu\beta_{nm}}{M} k_B T$, i.e., linearly proportional to the temperature and almost independent of the magnetic field (see also in Fig.S-3 in Suppl. [40]).

B. Thermal-magnetic shift on exciton energies

We now numerically investigate the thermal effect on energy by the Feranchuk-Komarov operator method [19, 50]. The obtained energies are given in Tab.S-II – Tab.S-VI in Suppl. [40] for the $1s$, $2s$, $3s$, $2p_{-1}$, and $2p_{+1}$ states. For an illustration of the effect, Figs. 2 (a) and (b) show exciton energies depending on the magnetic intensity at 0 K and 300 K.

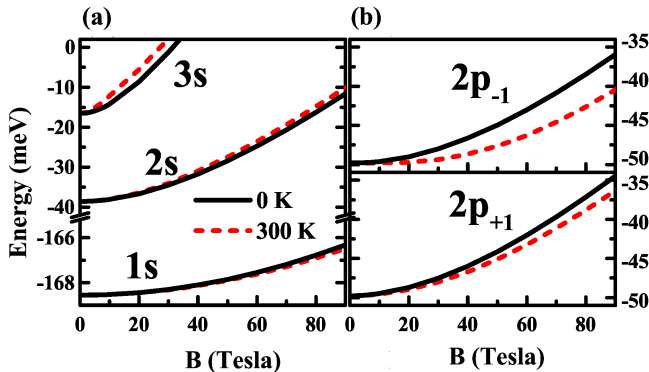


FIG. 2. (Color online) Exciton energies for the $1s$, $2s$, $3s$ (a), and $2p_{-1}$, $2p_{+1}$ (b) states depending on the magnetic intensity B at temperatures 0 K and 300 K.

We see that the temperature does not influence the $1s$ state much. At the same time, the thermal effect is noticeable for the $2s$ and higher Rydberg states for the magnetic intensity of more than 60 Tesla. Particularly for the magnetic intensity of 90 Tesla, the energy shifts when including the temperature of 300 K are shown in Table III. These shifts are big enough compared to the experimental sensitivity of 1 meV and are caused by the thermal motion of excitons in a magnetic field; thus, we call them the *thermal-magnetic shifts*.

We note that the thermal-magnetic shift predicted above is comparable with the shift caused by the phonon-

TABLE III. Thermal-magnetic shifts in exciton energy spectra calculated between the temperatures of 0 K and 300 K for the magnetic field of 90 Tesla.

	$1s$	$2s$	$3s$	$2p_{-1}$	$2p_{+1}$
ΔE (meV)	0.2	1.5	3.9	4.5	1.9

exciton interaction [24, 25]. For example, the polaron shift is about 15 meV at room temperature for $1s$ state exciton in the monolayer TMDC as shown in Ref. [25]. Compared with this, the thermal-magnetic shift for the $1s$ state, which is 0.2 meV as shown in Table III, can be ignored. It means that neglecting the exciton c.m. motion in Ref. [25] is feasible in this case. However, for a higher excited state such as $3s$, the thermal-magnetic shift of 3.9 meV should be taken into account if the polaron shift are calculated within the presence of a high magnetic field. The two shifts are from different mechanisms (phonon-exciton scattering versus the thermal motion of the exciton c.m. in a high magnetic field). They can be calculated separately, and both deserve consideration in analyzing experimental data for excited states in a high magnetic field. Also, for a high magnetic field of about 30 Tesla, as considered in Ref. [51], the fine structure energy split of excitons in monolayer TMDCs caused by the spin-magnetic interaction is up to tens of meV. Compared with this, the thermoinduced shift in the present paper is relatively noticeable, and it is important to consider.

C. Thermoinduced symmetry-breaking and enhancement of exciton lifetime

It is well-known that the system of a two-dimensional exciton in a magnetic field, perpendicular to the monolayer TMDC plane, has the potential energy dependent on radius $r = \sqrt{x^2 + y^2}$ only and consequently possesses the $SO(2)$ symmetry. However, if included, the thermo-reduced motional Stark potential (3), which depends on the angle φ as $\sim r \cos \varphi$, will break this symmetry. In this case, the angular momentum l_z is not conserved, and the magnetic number m is no longer a good quantum number. The consequence is that there are no true s states anymore, but only mixed states with $m \neq 0$ from the basis set functions; see Figs. 3 for the thermoinduced deformation of wave functions. More about the symmetry-breaking effect on the wave function deformation can be found in Sec.S-VIII C in Suppl. [40].

The wave function deformation leads to the change of the exciton radius, essential for the exciton radiative lifetime τ_{rad} , which is related to the average electron-hole distance $\langle r \rangle$ by the scaling law $\tau_{rad} \sim \langle r \rangle^\xi$ [29, 35]. The scaling factor ξ mainly depends on the dimensionality of the exciton. We roughly take the value of $\xi \approx 3.5$ extracted by studying the exciton in hBN, diamond, and

silicon provided in Ref. [35].

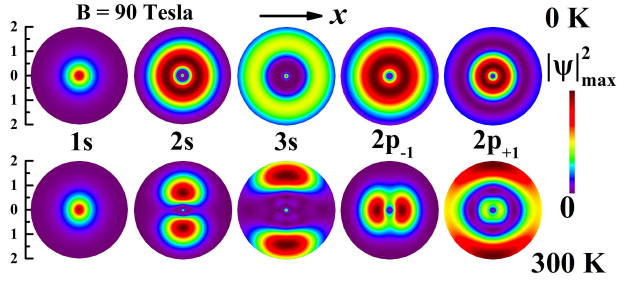


FIG. 3. (Color online) Deformation of wave functions due to the thermoinduced symmetry breaking.

To have an analytical estimation, we get the formula for the exciton radius of s states by the perturbation theory in the low magnetic field limit as

$$\langle r \rangle_T = \langle r \rangle + g e^2 B^2 \frac{k_B T}{M}, \quad (7)$$

where the radius $\langle r \rangle_T$ is calculated using the wave functions with thermal effect. In contrast, the free-field wave functions are used to calculate $\langle r \rangle$. The coefficient g has the following values 0.17×10^{-3} , 0.04, and -7.5 (nm^3/meV^2) for $1s$, $2s$, and $3s$ states, respectively. Consequently, we can get the following formula

$$\frac{\Delta \tau_{rad}}{\tau_{rad}} = \xi \frac{\Delta \langle r \rangle}{\langle r \rangle} \quad (8)$$

for the thermal correction $\Delta \tau_{rad}$ to the exciton radiative lifetime, where $\Delta \langle r \rangle = g e^2 B^2 \frac{k_B T}{M}$ for the low magnetic intensity. The correction $\Delta \langle r \rangle$ should be calculated numerically for the high magnetic field. We estimate the ratio (8) for the $1s$, $2s$, and $3s$ states at room temperature and magnetic field of 90 Tesla and get the following values: 1.4%, 4.9%, and 2.1%, relatively considerable. The thermoinduced correction to the radiative lifetime (8) qualitatively agrees with the first-principle calculations and experimental observations given in Refs. [31, 32, 34] for the $1s$ state, meaning that it always enhances the lifetime and is linearly proportional to the temperature. The thermal motion also causes the lifetime to be enhanced for the $2s$ state but reduced for the $3s$ state. Therefore, this effect (enhancement/reduction of the lifetime) needs further investigation for higher states in our next paper.

D. New peaks in absorption spectra due to the symmetry-breaking

Interestingly, the system's symmetry-breaking at room temperature can lead to new peaks in the magnetoexciton absorption spectra, as shown in Fig. 4. First, we calculate the imaginary part of the susceptibility by the

Elliot formula as

$$\alpha(\omega) = C \text{Im} \sum_{n,m} \frac{\omega |\psi_{nm}(\mathbf{r}=0)|^2}{E_{nm} + E_g - \hbar\omega + i\hbar\tau^{-1}} \quad (9)$$

based on the linear response theory of the exciton [52–55]. We use this quantity to estimate the absorption spectra since they are proportional. Here, the coefficient C depends on the materials' background refractive index and interband transition dipole matrix elements. We are only interested in the general picture and thus choose C to normalize the free-field $1s$ state peak to 1 and then use it as a constant for all other states.

In Eq. (9), the bandgap energy is taken by $E_g = 1890$ meV from the experiment [16]. For calculation at room temperature, we subtract a value of 65 meV from the bandgap, contributed by the Varshni and polaron shifts, based on the recent paper [25]. Besides, we also add the c.m. kinetic energy $K^2/2M$ of 51.8 meV to the relative energy to get the total exciton energy E_{nm} . Regarding the total lifetime, one usually considers both radiative and non-radiative dephasing effects as $1/\tau = 1/\tau_{rad} + 1/\tau_{non.rad}$. However, we roughly estimate the exciton lifetime τ by the scaling law $\tau_{rad} \sim \langle r \rangle^\xi$ [29, 35] and fit the coefficient from the experiment data for the $1s$ state [31], which suggests the exciton lifetime around 1 ps. The thermal correction to the lifetime based on the formula (8) of about a few percent is not noticeable in Fig. 4.

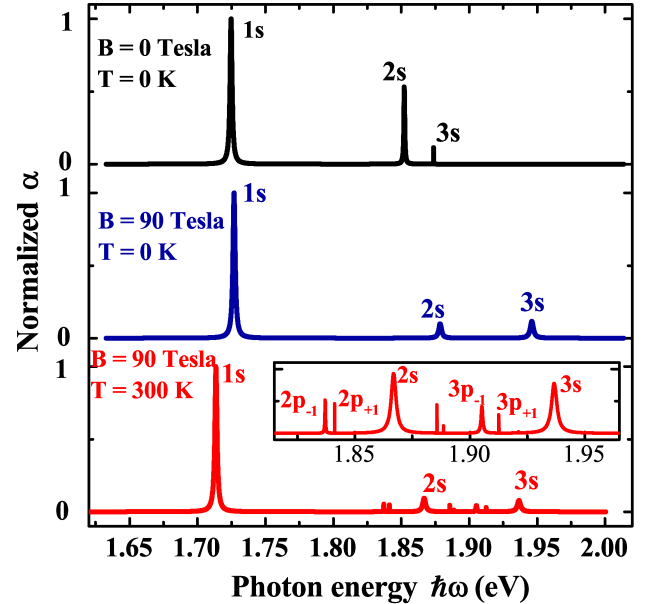


FIG. 4. (Color online) Normalized optical absorption spectra at temperature of 0 K (black and dark blue) and at room temperature (red).

Figure 4 illustrates the normalized linear optical absorption spectra for the quantum states with principal

quantum numbers $n < 4$. This qualitative picture shows the appearance of new peaks when considering the thermal effect. The explanation is based on the deformation of the wave functions, noting that the degeneracy lifting of the excited states and shifts of energies by the magnetic field and the thermoinduced potential also play an important role. Indeed, since the oscillation strength related to these peaks is proportional to the squared modulus of the wave functions at zero electron-hole separation, only the states associated with $|\psi_{nm}(\mathbf{r} = 0)|^2 \neq 0$ can be determined by the linear optical absorption spectrum. For zero-temperature magnetoexciton, only the s state wave functions have non-vanished oscillation strength while they vanish for all the other states such as p and d ; hence, we can only detect the exciton s states from the linear optical response, see Fig. 4 (black and dark blue lines). However, because of the thermal effect, the p and d states now become the superposition of other states, including s states. Therefore, we get the signal of the p - and d -state-exciton peaks on the linear optical absorption spectra at room temperature, as shown in Fig. 4 (red line). One can see more details about analytical examination of non- s -state peak emergence in Sec.S-VIII D in Suppl. [40].

IV. CONCLUSION

By separating the center of mass motion from an exciton in monolayer transition-metal dichalcogenide WSe_2 with a magnetic field, we have pointed out the thermoinduced motional Stark potential on the Schrödinger equation, which was previously neglected. Based on this, we have proposed a new mechanism that the thermal motion of the exciton c.m. in a magnetic field could affect the energy spectra of the magnetoexciton. As an observation

from our calculation, the thermal-magnetic shifts in the energy spectra are comparable with the polaron shifts caused by the exciton-phonon interaction, thus, should be considered for magnetoexciton energies at room temperature and can be observed by the shifts of resonance peaks on the absorption spectra. The thermoinduced potential also affects the diamagnetic coefficient and breaks the system's $\text{SO}(2)$ symmetry. The symmetry-breaking leads to the orbital deformation of the magnetoexciton that indirectly changes the exciton radiative lifetime, which can be observed by examining the width of the resonance peaks on the absorption spectra. Surprisingly, the system's symmetry-breaking at room temperature also causes the p -state exciton peaks to emerge on the linear optical absorption spectra, which cannot happen at zero temperature. These results provide another aspect of studying the influence of temperature on magnetoexciton and could be extended for other monolayer TMDCs such as WS_2 . As an outlook, this mechanism could be applied to trions, biexcitons in Dirac materials, and magnetoexcitons originating from the strain-induced pseudo-magnetic field.

ACKNOWLEDGMENTS

D.-N.Ly and N.-H.Phan are funded by Ho Chi Minh City University of Education Foundation for Science and Technology under grant numbers CS.2019.19.43TD and CS.2019.19.44TD. This paper is funded by Foundation for Science and Technology of Vietnam Ministry of Education and Training under grant number B2022-SPS-09-VL. This paper was carried out by the high-performance cluster at Ho Chi Minh City University of Education, Vietnam.

-
- [1] D.-N. Ly, D.-N. Le, N.-H. Phan, and V.-H. Le, Thermal effect on magnetoexciton energy spectra in monolayer transition metal dichalcogenides, *Phys. Rev. B* **107**, 155410 (2023).
- [2] T. C. Berkelbach, M. S. Hybertsen, and D. R. Reichman, Theory of neutral and charged excitons in monolayer transition metal dichalcogenides, *Phys. Rev. B* **88**, 045318 (2013).
- [3] A. Chernikov, T. C. Berkelbach, H. M. Hill, A. Rigosi, Y. Li, O. B. Aslan, D. R. Reichman, M. S. Hybertsen, and T. F. Heinz, Exciton binding energy and nonhydrogenic Rydberg series in monolayer WS_2 , *Phys. Rev. Lett.* **113**, 076802 (2014).
- [4] G. Wang, A. Chernikov, M. M. Glazov, T. F. Heinz, X. Marie, T. Amand, and B. Urbaszek, Colloquium: Excitons in atomically thin transition metal dichalcogenides, *Rev. Mod. Phys.* **90**, 021001 (2018).
- [5] M. R. Molas, A. O. Slobodeniuk, K. Nogajewski, M. Bartos, L. Bala, A. Babiński, K. Watanabe, T. Taniguchi, C. Faugeras, and M. Potemski, Energy spectrum of two-dimensional excitons in a nonuniform dielectric medium, *Phys. Rev. Lett.* **123**, 136801 (2019).
- [6] K. He, N. Kumar, L. Zhao, Z. Wang, K. F. Mak, H. Zhao, and J. Shan, Tightly bound excitons in monolayer WSe_2 , *Phys. Rev. Lett.* **113**, 026803 (2014).
- [7] M. M. Ugeda, A. J. Bradley, S.-F. Shi, F. H. da Jornada, Y. Zhang, D. Y. Qiu, W. Ruan, S.-K. Mo, Z. Hussain, Z.-X. Shen, F. Wang, S. G. Louie, and M. F. Crommie, Giant bandgap renormalization and excitonic effects in a monolayer transition metal dichalcogenide semiconductor, *Nature Materials* **13**, 1091 (2014).
- [8] Z. Ye, T. Cao, K. O'Brien, H. Zhu, X. Yin, Y. Wang, S. G. Louie, and X. Zhang, Probing excitonic dark states in single-layer tungsten disulphide, *Nature* **513**, 214 (2014).
- [9] H. M. Hill, A. F. Rigosi, C. Roquelet, A. Chernikov, T. C. Berkelbach, D. R. Reichman, M. S. Hybertsen, L. E. Brus, and T. F. Heinz, Observation of excitonic Rydberg states in monolayer MoS_2 and WS_2 by photoluminescence excitation spectroscopy, *Nano Letters* **15**, 2992 (2015).

- [10] A. Arora, M. Koperski, K. Nogajewski, J. Marcus, C. Faugeras, and M. Potemski, Excitonic resonances in thin films of WSe₂: from monolayer to bulk material, *Nanoscale* **7**, 10421 (2015).
- [1] A. Arora, T. Deilmann, T. Reichenauer, J. Kern, S. Michaelis de Vasconcellos, M. Rohlffing, and R. Bratschitsch, Excited-state trions in monolayer WS₂, *Phys. Rev. Lett.* **123**, 167401 (2019).
- [12] A. V. Stier, K. M. McCreary, B. T. Jonker, J. Kono, and S. A. Crooker, Exciton diamagnetic shifts and valley Zeeman effects in monolayer WS₂ and MoS₂ to 65 Tesla, *Nat. Commun.* **7**, 10643 (2016).
- [13] A. V. Stier, N. P. Wilson, G. Clark, X. Xu, and S. A. Crooker, Probing the influence of dielectric environment on excitons in monolayer WSe₂: Insight from high magnetic fields, *Nano Letters* **16**, 7054 (2016).
- [14] G. Plechinger, P. Nagler, A. Arora, A. Granados del Águila, M. V. Ballottin, T. Frank, P. Steinleitner, M. Gmitra, J. Fabian, P. C. M. Christianen, R. Bratschitsch, C. Schüller, and T. Korn, Excitonic valley effects in monolayer WS₂ under high magnetic fields, *Nano Letters* **16**, 7899 (2016).
- [15] M. Van der Donck, M. Zarenia, and F. M. Peeters, Excitons, trions, and biexcitons in transition-metal dichalcogenides: Magnetic-field dependence, *Phys. Rev. B* **97**, 195408 (2018).
- [16] A. V. Stier, N. P. Wilson, K. A. Velizhanin, J. Kono, X. Xu, and S. A. Crooker, Magneto-optics of exciton Rydberg states in a monolayer semiconductor, *Phys. Rev. Lett.* **120**, 057405 (2018).
- [17] J. Zipfel, J. Holler, A. A. Mitioglu, M. V. Ballottin, P. Nagler, A. V. Stier, T. Taniguchi, K. Watanabe, S. A. Crooker, P. C. M. Christianen, T. Korn, and A. Chernikov, Spatial extent of the excited exciton states in WS₂ monolayers from diamagnetic shifts, *Phys. Rev. B* **98**, 075438 (2018).
- [18] S.-Y. Chen, Z. Lu, T. Goldstein, J. Tong, A. Chaves, J. Kunstmann, L. S. R. Cavalcante, T. Woźniak, G. Seifert, D. R. Reichman, T. Taniguchi, K. Watanabe, D. Smirnov, and J. Yan, Luminescent emission of excited Rydberg excitons from monolayer WSe₂, *Nano Lett.* **19**, 2464 (2019).
- [19] D.-A. P. Nguyen, D.-N. Ly, D.-N. Le, N.-T. D. Hoang, and V.-H. Le, High-accuracy energy spectra of a two-dimensional exciton screened by reduced dimensionality with the presence of a constant magnetic field, *Physica E* **113**, 152 (2019).
- [20] E. Liu, J. van Baren, T. Taniguchi, K. Watanabe, Y.-C. Chang, and C. H. Lui, Magnetophotoluminescence of exciton Rydberg states in monolayer WSe₂, *Phys. Rev. B* **99**, 205420 (2019).
- [21] M. Goryca, J. Li, A. V. Stier, T. Taniguchi, K. Watanabe, E. Courtade, S. Shree, C. Robert, B. Urbaszek, X. Marie, and S. A. Crooker, Revealing exciton masses and dielectric properties of monolayer semiconductors with high magnetic fields, *Nat. Commun.* **10**, 4172 (2019).
- [22] R. Y. Kezerashvili and A. Spiridonova, Magnetoexcitons in transition metal dichalcogenides monolayers, bilayers, and van der Waals heterostructures, *Phys. Rev. Research* **3**, 033078 (2021).
- [23] D.-N. Ly, D.-N. Le, D.-A. P. Nguyen, N.-T. D. Hoang, N.-H. Phan, H.-M. L. Nguyen, and V.-H. Le, Retrieval of material properties of monolayer transition-metal dichalcogenides from magnetoexciton energy spectra (2023), [arXiv:2303.08089](https://arxiv.org/abs/2303.08089) [cond-mat.mes-hall].
- [24] F. Lengers, T. Kuhn, and D. E. Reiter, Phonon signatures in spectra of exciton polaritons in transition metal dichalcogenides, *Phys. Rev. B* **104**, L241301 (2021).
- [25] J. C. G. Henriques and N. M. R. Peres, Perturbative approach to the polaron shift of excitons in transition metal dichalcogenides, *Phys. Rev. B* **103**, L161402 (2021).
- [26] N.-T. D. Hoang, D.-N. Ly, and V.-H. Le, Comment on “Excitons, trions, and biexcitons in transition-metal dichalcogenides: Magnetic-field dependence”, *Phys. Rev. B* **101**, 127401 (2020).
- [27] J. E. Avron, I. W. Herbst, and B. Simon, Separation of center of mass in homogeneous magnetic fields, *Annals of Physics* **114**, 431 (1978).
- [28] H. Ruder, G. Wunner, H. Herold, and F. Geyer, *Atoms in Strong Magnetic Fields* (Springer - Verlag, Berlin, 1994).
- [29] Y. Toyozawa, *Optical Processes in Solids* (Cambridge University Press, 2003) p. 422.
- [30] A. Chernikov, V. Bornwasser, M. Koch, S. Chatterjee, C. N. Böttge, T. Feldtmann, M. Kira, S. W. Koch, T. Wassner, S. Lautenschläger, B. K. Meyer, and M. Eickhoff, Phonon-assisted luminescence of polar semiconductors: Fröhlich coupling versus deformation-potential scattering, *Phys. Rev. B* **85**, 035201 (2012).
- [31] M. Palummo, M. Bernardi, and J. C. Grossman, Exciton radiative lifetimes in two-dimensional transition metal dichalcogenides, *Nano Letters* **15**, 2794 (2015).
- [32] M. Selig, G. Berghäuser, A. Raja, P. Nagler, C. Schüller, T. F. Heinz, T. Korn, A. Chernikov, E. Malic, and A. Knorr, Excitonic linewidth and coherence lifetime in monolayer transition metal dichalcogenides, *Nat. Commun.* **7**, 13279 (2016).
- [33] D. Van Tuan, M. Yang, and H. Dery, Coulomb interaction in monolayer transition-metal dichalcogenides, *Phys. Rev. B* **98**, 125308 (2018).
- [34] S. Brem, J. Zipfel, M. Selig, A. Raja, L. Waldecker, J. D. Ziegler, T. Taniguchi, K. Watanabe, A. Chernikov, and E. Malic, Intrinsic lifetime of higher excitonic states in tungsten diselenide monolayers, *Nanoscale* **11**, 12381 (2019).
- [35] Roux, Sébastien and Arnold, Christophe and Paleari, Fulvio and Sponza, Lorenzo and Janzen, Eli and Edgar, James H. and Toury, Bérangère and Journet, Catherine and Garnier, Vincent and Steyer, Philippe and Taniguchi, Takashi and Watanabe, Kenji and Ducastelle, François and Loiseau, Annick and Barjon, Julien, Radiative lifetime of free excitons in hexagonal boron nitride, *Phys. Rev. B* **104**, L161203 (2021).
- [36] N. S. Rytova, Screened potential of a point charge in a thin film, *Mosc. Univ. Phys. Bull.* **22**, 30 (1967).
- [37] L. V. Keldysh, Coulomb interaction in thin semiconductor and semimetal films, *JETP Lett.* **29**, 658 (1979).
- [38] P. Cudazzo, I. V. Tokatly, and A. Rubio, Dielectric screening in two-dimensional insulators: Implications for excitonic and impurity states in graphene, *Phys. Rev. B* **84**, 085406 (2011).
- [39] E. Hanamura, N. Nagaosa, M. Kumagai, and T. Takagahara, Quantum wells with enhanced exciton effects and optical non-linearity, *Mater. Sci. Eng. B* **1**, 255 (1988).
- [40] See Supplemental Materials for detailed derivations of the Separation of center-of-mass motion, Thermo-induced motional potential, Feranchuk-Komarov operator method for magnetoexciton energies, Analysis of

- thermo-induced effect by the perturbation method with additional references [56–58].
- [1] C. Poellmann, P. Steinleitner, U. Leierseder, P. Nagler, G. Plechinger, M. Porer, R. Bratschitsch, C. Schüller, T. Korn, and R. Huber, Resonant internal quantum transitions and femtosecond radiative decay of excitons in monolayer WSe₂, *Nature Materials* **14**, 889 (2015).
- [42] T. Yan, X. Qiao, P. Tan, and X. Zhang, Valley depolarization in monolayer WSe₂, *Scientific Reports* **5**, 15625 (2015).
- [43] Y. You, X.-X. Zhang, T. C. Berkelbach, M. S. Hybertsen, D. R. Reichman, and T. F. Heinz, Observation of biexcitons in monolayer WSe₂, *Nature Physics* **11**, 477 (2015).
- [44] P. Steinleitner, P. Merkl, P. Nagler, J. Mornhinweg, C. Schüller, T. Korn, A. Chernikov, and R. Huber, Direct observation of ultrafast exciton formation in a monolayer of WSe₂, *Nano Letters* **17**, 1455 (2017).
- [45] D. Farrelly, Motional Stark effect on Rydberg states in crossed electric and magnetic fields, *Physics Letters A* **191**, 265 (1994).
- [46] F. Schweiner, P. Rommel, J. Main, and G. Wunner, Exciton-phonon interaction breaking all antiunitary symmetries in external magnetic fields, *Phys. Rev. B* **96**, 035207 (2017).
- [47] K. Tanaka, M. Kobashi, T. Shichiri, T. Yamabe, D. M. Silver, and H. J. Silverstone, LoSurdo-Stark effect for a hydrogenic impurity in a thin layer: Two-dimensional model, *Phys. Rev. B* **35**, 2513 (1987).
- [48] J. C. G. Henriques, H. C. Kamban, T. G. Pedersen, and N. M. R. Peres, Analytical quantitative semiclassical approach to the LoSurdo–Stark effect and ionization in two-dimensional excitons, *Phys. Rev. B* **102**, 035402 (2020).
- [49] H. C. Kamban and T. G. Pedersen, Field-induced dissociation of two-dimensional excitons in transition metal dichalcogenides, *Phys. Rev. B* **100**, 045307 (2019).
- [50] I. Feranchuk, A. Ivanov, V.-H. Le, and A. Ulyanov, *Non-perturbative Description of Quantum Systems* (Springer, Switzerland, 2015).
- [51] C. Robert, B. Han, P. Kapuscinski, A. Delhomme, C. Faugeras, T. Amand, M. R. Molas, M. Bartos, K. Watanabe, T. Taniguchi, B. Urbaszek, M. Potemski, and X. Marie, Measurement of the spin-forbidden dark excitons in MoS₂ and MoSe₂ monolayers, *Nat. Commun.* **11**, 4037 (2020).
- [52] M. Kira and S. Koch, Many-body correlations and excitonic effects in semiconductor spectroscopy, *Progress in Quantum Electronics* **30**, 155 (2006).
- [53] H. Haug and S. W. Koch, *Quantum Theory of the Optical and Electronic Properties of Semiconductors*, 5th ed. (World Scientific, 2009).
- [54] S. Wu, L. Cheng, and Q. Wang, Exciton states and absorption spectra in freestanding monolayer transition metal dichalcogenides: A variationally optimized diagonalization method, *Phys. Rev. B* **100**, 115430 (2019).
- [55] S. Wu, Anisotropic exciton states and excitonic absorption spectra in a freestanding monolayer black phosphorus, *Physica E* **141**, 115238 (2022).
- [56] A. P. Prudnikov, Y. A. Brychkov, and O. I. Marichev, *Integrals and Series*, Vol. 5: Inverse Laplace Transforms (Gordon and Breach Science Publishers, New York, 1992).
- [57] L. V. Hoang and N. T. Giang, The algebraic method for two-dimensional quantum atomic systems, *J. Phys. A: Math. Gen.* **26**, 1409 (1993).
- [58] Netlib.org. LAPACK: Linear Algebra PACKage, Subroutine dsygvx.f.

Supplemental materials for:
**Thermal effect on magnetoexciton energy spectra in monolayer
transition-metal dichalcogenides**

Duy-Nhat Ly ^{1,†}, Dai-Nam Le ^{2,†}, Ngoc-Hung Phan ¹ and Van-Hoang Le ¹

¹*Computational Physics Key Laboratory K002, Department of Physics, Ho Chi Minh City University of Education,
Ho Chi Minh City 72759, Vietnam*

²*Department of Physics, University of South Florida, Tampa, Florida 33620, USA*

[†]*These authors contributed equally to this work.*

Emails: nhatld@hcmue.edu.vn (D.-N. Ly), dainamle@usf.edu (D.-N. Le), hoanglv@hcmue.edu.vn (V.-H. Le).

Links: <http://link.aps.org/supplemental/10.1103/PhysRevB.107.155410>.

CONTENTS

I.	Introduction	1
II.	Theoretical background	2
	A. Schrödinger equation	2
	B. Thermoinduced motional Stark potential	2
III.	Results and Discussion	3
	A. Thermal effect on diamagnetic coefficient and Landau levels	3
	B. Thermal-magnetic shift on exciton energies	4
	C. Thermoinduced symmetry-breaking and enhancement of exciton lifetime	4
	D. New peaks in absorption spectra due to the symmetry-breaking	5
IV.	Conclusion	6
	acknowledgments	6
	References	6
S-V.	Separation of center-of-mass motion	S-2
	A. Hamiltonian for an electron-hole system in a magnetic field	S-2
	B. Pseudomomentum of the electron-hole system in a magnetic field	S-2
	C. Variable-separation and the Hamiltonian for the relative motion	S-3
S-VI.	Thermo-induced motional Stark potential	S-4
S-VII.	Feranchuk-Komarov operator method for magnetoexciton energies under influence of thermo-induced Stark potential	S-6
	A. Schrödinger equation in the formalism of creation and annihilation operators	S-6
	B. Matrix elements	S-8
	C. Exciton energy spectrum for magnetoexciton in WSe ₂ monolayer at zero and room temperatures	S-9
S-VIII.	Analysis of thermo-induced effect by the perturbation method	S-12
	A. In low magnetic field intensity limit	S-13
	B. In high magnetic field intensity limit	S-14
	C. Thermo-induced deformation of magnetoexciton wave functions by symmetry-breaking mechanism	S-15
	D. Squared modulus of magnetoexciton wave functions at zero separation of electron-hole pair for <i>np</i> and <i>nd</i> states	S-18
	References	S-19

S-V. SEPARATION OF CENTER-OF-MASS MOTION

A. Hamiltonian for an electron-hole system in a magnetic field

The Hamiltonian for an electron-hole system in a magnetic field can be written as

$$\hat{H}_{ex} = \frac{1}{2m_e^*} \hat{\mathbf{P}}_e^2 + \frac{1}{2m_h^*} \hat{\mathbf{P}}_h^2 + \frac{eB}{2m_e^*} \hat{l}_z^e - \frac{eB}{2m_h^*} \hat{l}_z^h + \frac{e^2 B^2}{8m_e^*} r_e^2 + \frac{e^2 B^2}{8m_h^*} r_h^2 + \hat{V}_{h-e}(|\mathbf{r}_h - \mathbf{r}_e|), \quad (\text{S-1})$$

where m_e^* and m_h^* are the effective masses of the electron and hole, respectively. To separate the variables, we use the center of mass (c.m.) coordinates $\mathbf{R} = X \mathbf{i} + Y \mathbf{j}$ and the relative coordinates $\mathbf{r} = x \mathbf{i} + y \mathbf{j}$ defined by the transformation

$$\begin{aligned} X &= \frac{m_h^*}{m_h^* + m_e^*} x_h + \frac{m_e^*}{m_h^* + m_e^*} x_e, & x &= x_e - x_h, \\ Y &= \frac{m_h^*}{m_h^* + m_e^*} y_h + \frac{m_e^*}{m_h^* + m_e^*} y_e, & y &= y_e - y_h. \end{aligned} \quad (\text{S-2})$$

For the separation, we need to rewrite all the terms in Hamiltonian (S-1) in the coordinates (\mathbf{r}, \mathbf{R}) and, as a result, obtain the following

$$\frac{1}{2m_e^*} \hat{\mathbf{p}}_e^2 + \frac{1}{2m_h^*} \hat{\mathbf{p}}_h^2 = \frac{1}{2M} \hat{\mathbf{P}}^2 + \frac{1}{2\mu} \hat{\mathbf{p}}^2, \quad (\text{S-3})$$

$$\frac{eB}{2m_e^*} \hat{l}_z^e - \frac{eB}{2m_h^*} \hat{l}_z^h = \frac{1-\sigma}{1+\sigma} \frac{eB}{2\mu} \hat{l}_z + \frac{e}{2M} (\mathbf{B} \times \mathbf{r}) \cdot \hat{\mathbf{P}} + \frac{e}{2\mu} (\mathbf{B} \times \mathbf{R}) \cdot \hat{\mathbf{p}}, \quad (\text{S-4})$$

$$\frac{1}{m_e^*} r_e^2 + \frac{1}{m_h^*} r_h^2 = \frac{1}{\mu} R^2 + \frac{1-\sigma}{(1+\sigma)\mu} 2\mathbf{r} \cdot \mathbf{R} + \left(\frac{1}{\mu} - \frac{3}{M} \right) r^2. \quad (\text{S-5})$$

Here, the total mass M , the reduced mass μ , and the ratio of masses σ are defined as

$$M = m_h^* + m_e^*, \quad \frac{1}{\mu} = \frac{1}{m_e^*} + \frac{1}{m_h^*}, \quad \sigma = m_e^*/m_h^*; \quad (\text{S-6})$$

$\hat{\mathbf{P}}$ is the c.m. momentum; $\hat{\mathbf{p}}$ is the momentum of the relative motion between the electron and hole; $\hat{l}_z = x\hat{p}_y - y\hat{p}_x$ is the angular momentum of the relative motion on Oxy plane.

Using equations (S-3), (S-4), and (S-5), we can rewrite the Hamiltonian in the coordinate system of the c.m. as

$$\begin{aligned} \hat{H}_{ex} &= \frac{1}{2\mu} \hat{\mathbf{p}}^2 + \frac{1-\sigma}{1+\sigma} \frac{eB}{2\mu} \hat{l}_z + \frac{M-3\mu}{M\mu} \frac{e^2 B^2}{8} r^2 + \hat{V}_{h-e}(r) \\ &+ \frac{1}{2M} \hat{\mathbf{P}}^2 + \frac{e^2 B^2}{8\mu} R^2 + \frac{e^2 B^2}{4\mu} \frac{1-\sigma}{1+\sigma} \mathbf{r} \cdot \mathbf{R} \\ &+ \frac{e}{2M} (\mathbf{B} \times \mathbf{r}) \cdot \hat{\mathbf{P}} + \frac{e}{2\mu} (\mathbf{B} \times \mathbf{R}) \cdot \hat{\mathbf{p}}. \end{aligned} \quad (\text{S-7})$$

B. Pseudomomentum of the electron-hole system in a magnetic field

At first sight, Hamiltonian (S-7) is not variable-separable for the coordinates \mathbf{R} and \mathbf{r} because the total momentum $\hat{\mathbf{P}}$ is not conserved. However, there is another conservative quantity for the considered system [1–3], called pseudomomentum, defined as

$$\hat{\mathbf{P}}_0 = \hat{\mathbf{P}} - \frac{1}{2} e\mathbf{B} \times \mathbf{r}. \quad (\text{S-8})$$

We will insert this vector in the Hamiltonian instead of $\hat{\mathbf{P}}$. For this purpose, we first calculate the quadratic form $\hat{\mathbf{P}}_0^2$ and then express the kinetic energy operator of c.m. via $\hat{\mathbf{P}}_0$ as

$$\frac{1}{2M} \hat{\mathbf{P}}^2 = \frac{1}{2M} \hat{\mathbf{P}}_0^2 + \frac{e}{2M} (\mathbf{B} \times \mathbf{r}) \cdot \hat{\mathbf{P}}_0 + \frac{e^2 B^2}{8M} r^2. \quad (\text{S-9})$$

The other term in the Hamiltonian containing the total momentum $\hat{\mathbf{P}}$ can be expressed via $\hat{\mathbf{P}}_0$ too,

$$\frac{e}{2M}(\mathbf{B} \times \mathbf{r}) \cdot \hat{\mathbf{P}} = \frac{e}{2M}(\mathbf{B} \times \mathbf{r}) \cdot \hat{\mathbf{P}}_0 + \frac{e^2 B^2}{4M} r^2. \quad (\text{S-10})$$

Using equations (S-9) and (S-10), we rewrite the Hamiltonian (S-7) into

$$\begin{aligned} \hat{H}_{ex} &= \frac{1}{2\mu} \hat{\mathbf{p}}^2 + \frac{1 - \sigma eB}{1 + \sigma} \frac{eB}{2\mu} \hat{l}_z + \frac{e^2 B^2}{8\mu} r^2 + \hat{V}_{h-e}(r) \\ &+ \frac{1}{2M} \hat{\mathbf{P}}_0^2 + \frac{e}{M} (\mathbf{B} \times \mathbf{r}) \cdot \hat{\mathbf{P}}_0 + \frac{e^2 B^2}{8\mu} R^2 + \frac{1 - \sigma e^2 B^2}{1 + \sigma} \frac{e^2 B^2}{4\mu} \mathbf{r} \cdot \mathbf{R} + \frac{e}{2\mu} (\mathbf{B} \times \mathbf{R}) \cdot \hat{\mathbf{p}}, \end{aligned} \quad (\text{S-11})$$

which now contains \mathbf{P}_0 only.

We can also confirm that the pseudomomentum $\hat{\mathbf{P}}_0$ commutes with the Hamiltonian (S-11) by calculating commutators of $\hat{\mathbf{P}}_0$ with all the Hamiltonian terms. The following commutator relations

$$\left[\hat{\mathbf{P}}_0, \frac{e^2 B^2}{8\mu} r^2 \right] = 0, \quad \left[\hat{\mathbf{P}}_0, \hat{V}_{h-e}(r) \right] = 0, \quad \left[\hat{\mathbf{P}}_0, \frac{e}{M} (\mathbf{B} \times \mathbf{r}) \cdot \hat{\mathbf{P}}_0 \right] = 0 \quad (\text{S-12})$$

are trivially obtained because the operator $\hat{\mathbf{P}}_0$ does not contain the differential operator respecting \mathbf{r} . For all other terms in the Hamiltonian, we can calculate and receive the following commutators

$$\begin{aligned} \left[\hat{\mathbf{P}}_0, \hat{\mathbf{p}}^2 \right] &= -i\hbar e\mathbf{B} \times \hat{\mathbf{p}}, \quad \left[\hat{\mathbf{P}}_0, \hat{l}_z \right] = \frac{1}{2} i\hbar eB \mathbf{r}, \quad \left[\hat{\mathbf{P}}_0, R^2 \right] = -\frac{1}{2} i\hbar \mathbf{R}, \\ \left[\hat{\mathbf{P}}_0, \mathbf{r} \cdot \mathbf{R} \right] &= -i\hbar \mathbf{r}, \quad \left[\hat{\mathbf{P}}_0, (e\mathbf{B} \times \mathbf{R}) \cdot \hat{\mathbf{p}} \right] = i\hbar e\mathbf{B} \times \hat{\mathbf{p}} + \frac{1}{2} i\hbar e^2 B^2 \mathbf{R}. \end{aligned} \quad (\text{S-13})$$

From equations (S-12) and (S-13), we can prove

$$\left[\hat{\mathbf{P}}_0, \hat{H}_{ex} \right] = 0, \quad (\text{S-14})$$

meaning that $\hat{\mathbf{P}}_0$ is an integral of motion, and $\hat{\mathbf{P}}_0$ and \hat{H}_{ex} have mutual eigenfunctions.

C. Variable-separation and the Hamiltonian for the relative motion

We will use eigenfunctions of the pseudomomentum $\hat{\mathbf{P}}_0$ to separate the variables in the total Hamiltonian (S-7). For the first move, it is easy to verify that the wave function

$$\Psi(\mathbf{R}, \mathbf{r}) = \exp \left\{ \frac{i}{\hbar} \left(\mathbf{K} + \frac{e}{2} \mathbf{B} \times \mathbf{r} \right) \cdot \mathbf{R} \right\} \psi(\mathbf{r}) \quad (\text{S-15})$$

is an eigenfunction of the operator $\hat{\mathbf{P}}_0$ with an eigenvector \mathbf{K} , i. e., satisfies the eigenvalue equation

$$\hat{\mathbf{P}}_0 \Psi(\mathbf{R}, \mathbf{r}) = \mathbf{K} \Psi(\mathbf{R}, \mathbf{r}). \quad (\text{S-16})$$

Because of the commutation relation $\left[\hat{\mathbf{P}}_0, \hat{H}_{ex} \right] = 0$, we can choose $\psi(\mathbf{r})$ so that the wave function $\Psi(\mathbf{R}, \mathbf{r})$ becomes an eigenfunction of the Hamiltonian \hat{H}_{ex} , i. e.,

$$\hat{H}_{ex} \Psi(\mathbf{R}, \mathbf{r}) = E_{total} \Psi(\mathbf{R}, \mathbf{r}). \quad (\text{S-17})$$

Denoting $\hat{U} = \exp \left\{ \frac{i}{\hbar} \left(\mathbf{K} + \frac{e}{2} \mathbf{B} \times \mathbf{r} \right) \cdot \mathbf{R} \right\}$, we can rewrite equation (S-17) into

$$\hat{H}_{ex} \hat{U} \psi(\mathbf{r}) = E_{total} \hat{U} \psi(\mathbf{r}) \rightarrow \hat{U}^{-1} \hat{H}_{ex} \hat{U} \psi(\mathbf{r}) = E_{total} \psi(\mathbf{r}). \quad (\text{S-18})$$

The function $\psi(\mathbf{r})$, depending only on \mathbf{r} , can be considered as a wave function of the electron-hole relative motion. Consequently, equation (S-18) (subtracted by the pseudokinetic energy of the exciton c.m.) is the Schrödinger equation for relative motion with the Hamiltonian defined by the transformation

$$\hat{H}_{rel} = \hat{U}^{-1} \hat{H}_{ex} \hat{U} - \frac{1}{2M} K^2 \quad (\text{S-19})$$

with the relative energy $E = E_{total} - \frac{1}{2M}K^2$.

We can directly calculate all the terms of the Hamiltonian \hat{H}_{rel} with the following results

$$\begin{aligned}\hat{U}^{-1}\hat{\mathbf{p}}^2\hat{U} &= \hat{\mathbf{p}}^2 - (e\mathbf{B} \times \mathbf{R}) \cdot \hat{\mathbf{p}} + \frac{1}{4}e^2B^2R^2, \\ \hat{U}^{-1}(e\mathbf{B} \times \mathbf{R}) \cdot \hat{\mathbf{p}}\hat{U} &= -\frac{1}{2}e^2B^2R^2 + (e\mathbf{B} \times \mathbf{R}) \cdot \hat{\mathbf{p}}, \\ \hat{U}^{-1}\hat{l}_z\hat{U} &= \hat{l}_z - \frac{1}{2}eB\mathbf{r} \cdot \mathbf{R}, \quad \hat{U}^{-1}\hat{\mathbf{P}}_0^2\hat{U} = K^2, \quad \hat{U}^{-1}(e\mathbf{B} \times \mathbf{r}) \cdot \hat{\mathbf{P}}_0\hat{U} = (e\mathbf{B} \times \mathbf{K}) \cdot \mathbf{r}, \\ \hat{U}^{-1}r^2\hat{U} &= r^2, \quad \hat{U}^{-1}\hat{V}_{h-e}(r)\hat{U} = \hat{V}_{h-e}(r), \quad \hat{U}^{-1}R^2\hat{U} = R^2, \quad \hat{U}^{-1}\mathbf{r} \cdot \mathbf{R}\hat{U} = \mathbf{r} \cdot \mathbf{R}.\end{aligned}\quad (\text{S-20})$$

From equations (S-19) and (S-20), we obtain the Hamiltonian for the relative motion between the electron and the hole as

$$\hat{H}_{rel} = \frac{1}{2\mu}\hat{\mathbf{p}}^2 + \frac{1-\sigma}{1+\sigma}\frac{eB}{2\mu}\hat{l}_z + \frac{e^2B^2}{8\mu}r^2 + \hat{V}_{h-e}(r) - \frac{e}{M}(\mathbf{B} \times \mathbf{K}) \cdot \mathbf{r}, \quad (\text{S-21})$$

which is the Hamiltonian in equation (2) of the main text.

S-VI. THERMO-INDUCED MOTIONAL STARK POTENTIAL

In equation (S-21), we now consider the term

$$V_{mS}(\mathbf{r}) = -\frac{e}{M}(\mathbf{B} \times \mathbf{K}) \cdot \mathbf{r}, \quad (\text{S-22})$$

which was neglected in the previous works for the exciton energies in monolayer TMDCs. The term (S-22) contains the exciton c.m. pseudomomentum \mathbf{K} that inspires us to establish its relation to the thermal motion of excitons in a monolayer TMDC.

Excitons in a monolayer TMDC can be regarded as a gas of thermal motion with kinetic energy $K^2/2M$. We first compare the average distance between two excitons $\lambda_{ex} = 1/\sqrt{n_X}$ with the thermal wavelength $\lambda_{th} = \sqrt{2\pi\hbar^2/(Mk_B T)}$ to justify which statistics should be applied for the kinetic energy distribution. Here, n_X is the exciton density – the number of neutral excitons per unit of area; k_B is the Boltzmann constant. For the Maxwell-Boltzmann statistics to be applied, the thermal wavelength should be much smaller than the average exciton distance that leads to the limit for the exciton density as

$$\lambda_{th} \ll \lambda_{ex} \rightarrow n_X \ll n_{max} = \frac{Mk_B T}{2\pi\hbar^2}. \quad (\text{S-23})$$

For room temperature, 300K, we calculate the limit for the exciton density in monolayer WSe₂ where $M = 0.8 \times m_e$ and receive a result $n_{max-300K} = 4.3 \times 10^{12}\text{cm}^{-2}$. On another side, the exciton density is modulated around 10^{11} – 10^{12}cm^{-2} in real experiments for monolayer WSe₂ [4–7], which is much smaller than its limit $n_{max-300K}$ at room temperature. Therefore, we can estimate the root-mean-square of the c.m. pseudomomentum at temperature T by the equipartition theorem as $\frac{1}{2M}\overline{K^2} = k_B T$.

In exciton gas, pseudomomentum K has an assembly of values (K_1, K_2, \dots) obeyed the Maxwell-Boltzmann distribution. To obtain the average energy \overline{E} of different values K , we principally need to calculate energies for each value K_j and then average the calculated energies. However, we can do this in another way by calculating energy at the average pseudomomentum $\overline{K} = \sqrt{\overline{K^2}}$. The results must be the same $E(\overline{K}) \simeq \overline{E}$. The base for this assumption is the perturbation theory calculation that the thermo-induced potential leads to a small correction to the energy, which is proportional to the quantity K^2 as $E = E^{(0)} + b \times K^2$ so that $\overline{E} = E^{(0)} + b \times \overline{K^2}$. We also verify numerically that the two average methods (the average energy by different pseudomomentum vs. the energy at the average pseudomomentum) give the same results presented in Table S-I with diminutive differences of about 0.1 meV, except for 3s-state with about 0.5 meV difference (relative error of 0.68%).

Consequently, from the above discussion, we can estimate the average pseudomomentum of exciton c.m. motion via temperature and rewrite the motional stark potential in the form

$$V_{mS}(\mathbf{r}) = -\sqrt{\frac{2k_B T}{M}}eBx. \quad (\text{S-24})$$

Here, without losing generality, we consider the case where \mathbf{K} is along the Oy axis so that vector $\mathbf{B} \times \mathbf{K}$ is along the Ox axis.

For the system of an atom in external electric and magnetic field, the consideration of the term (S-21) leads to additional contribution in the Stark effect although being originated from the magnetic field; thus called the motional Stark effect [8, 9]. However, because this term is related to the thermal motion as we shown via the formula (S-24), we call it the thermo-induced motional Stark potential.

The effective potential in Hamiltonian (S-21) consists of three terms as $\hat{V}_{eff} = \hat{V}_{diamag} + \hat{V}_{h-e} + \hat{V}_{mS}$, where the diamagnetic term $V_{diamag.}(\mathbf{r}) = \frac{e^2 B^2}{8\mu} r^2$ is quadratic proportional to the electron-hole distance and consequently dominant at the large separation of the electro-hole pair compared to the thermo-induced motional Stark term \hat{V}_{mS} , which is linearly proportional to the variable x . As a result, there is no tunneling effect, even considering the thermo-induced motional Stark potential. Instead of tunneling, we expect the thermo-induced motional Stark potential causes the Stark shift in the energy spectra. This fact is also demonstrated clearly in Fig. S-1, where the inclusion of the thermal effect causes a higher raising in the effective potential.

TABLE S-I. Exciton energies (meV) in the magnetic field of 90 Tesla with different values of K^2 calculated for monolayer WSe₂ with $r_0 = 4.2086$ nm, $\mu = 0.2039 m_e$, $\kappa = 4.5$. It also indicates energies averaged by K^2 and calculated at the average value of K^2 . The energy differences between the two different calculation methods are in the last row.

K (\hbar/a_0) $\times 10^{-3}$	K^2 (\hbar^2/a_0^2) $\times 10^{-3}$	Energy (meV)				
		1s	2p ₋₁	2p ₊₁	2s	3s
0	0	-165.807	-33.280	-31.645	-6.750	68.124
5	0.025	-165.808	-33.292	-31.657	-6.743	68.148
10	0.100	-165.810	-33.329	-31.693	-6.721	68.221
15	0.225	-165.813	-33.390	-31.752	-6.684	68.339
20	0.400	-165.818	-33.479	-31.831	-6.634	68.501
25	0.625	-165.824	-33.597	-31.927	-6.570	68.700
30	0.900	-165.831	-33.748	-32.037	-6.495	68.934
35	1.225	-165.839	-33.934	-32.157	-6.408	69.195
40	1.600	-165.849	-34.158	-32.285	-6.312	69.478
45	2.025	-165.860	-34.420	-32.417	-6.207	69.777
50	2.500	-165.872	-34.722	-32.552	-6.094	70.086
55	3.025	-165.886	-35.062	-32.690	-5.977	70.397
60	3.600	-165.901	-35.439	-32.831	-5.855	70.706
65	4.225	-165.917	-35.852	-32.976	-5.732	71.004
70	4.900	-165.935	-36.299	-33.125	-5.608	71.284
75	5.625	-165.954	-36.779	-33.280	-5.485	71.538
80	6.400	-165.974	-37.288	-33.440	-5.365	71.757
85	7.225	-165.995	-37.827	-33.608	-5.251	71.928
90	8.100	-166.018	-38.394	-33.782	-5.144	72.036
95	9.025	-166.042	-38.987	-33.965	-5.046	72.060
100	10.000	-166.068	-39.605	-34.156	-4.961	71.977
Average	3.417	-165.896	-35.375	-32.657	-6.002	70.104
	$E(K^2 = 3.417)$	-165.895	-35.284	-32.774	-5.904	70.580
	Difference (meV)	0.001	0.091	0.117	0.098	0.479

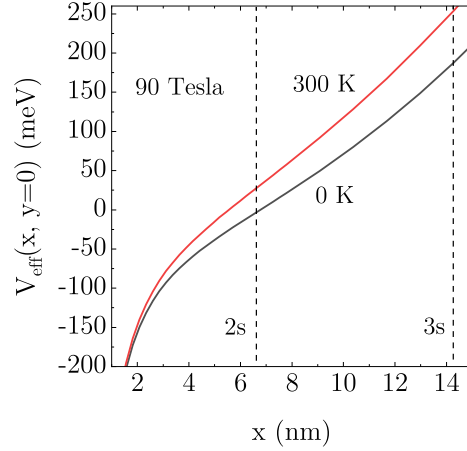


FIG. S-1. The effective potentials for relative motion in two cases: $T = 0K$ (black) and $T = 300K$ (red), i.e., without and with the motional Stark term. The difference between the potentials is noticeable for $2s$ and higher Rydberg states, where the exciton radius is larger than 6.5 nm.

S-VII. FERANCHUK-KOMAROV OPERATOR METHOD FOR MAGNETOEXCITON ENERGIES UNDER INFLUENCE OF THERMO-INDUCED STARK POTENTIAL

A. Schrödinger equation in the formalism of creation and annihilation operators

Magnetoexciton under the influence of thermo-induced Stark potential is described by the Schrödinger equation (2) in the main text. We rewrite it in a dimensionless form where the energy E and the coordinates x, y are given in the effective Hartree unit $2Ry^* = \mu e^4 / 16\pi^2 \epsilon_0^2 \hbar^2$ and the effective Bohr radius $a_0^* = 4\pi\epsilon_0 \hbar^2 / \mu e^2$, respectively; the dimensionless magnetic intensity γ is related to the magnetic field by the equation $B = 2\gamma \times \mu \hbar Ry^* / e$. Then the Levi-Civita transformation [10]

$$x = u^2 - v^2, \quad y = 2uv \quad (\text{S-25})$$

is applied to the dimensionless Schrödinger equation to rewrite it in the (u, v) space as

$$\left\{ -\frac{1}{8} \left(\frac{\partial^2}{\partial u^2} + \frac{\partial^2}{\partial v^2} \right) + \left(\frac{1 - \sigma \gamma}{1 + \sigma} \frac{\hat{l}_z}{2} - E \right) (u^2 + v^2) + \frac{\gamma^2}{8} (u^2 + v^2)^3 + \frac{\sqrt{2\sigma\theta}}{1 + \sigma} \gamma (u^4 - v^4) + V(u, v) \right\} \psi(u, v) = 0, \quad (\text{S-26})$$

where $\theta = k_B T / 2Ry^*$ is dimensionless temperature; and $V(u, v) = (u^2 + v^2) V_{RK}$. Here, from now on, we use the notation V_{RK} for the interaction potential of the electron and hole \hat{V}_{h-e} . Also, for convenience in calculations, we rewrite the potential $V(u, v)$ in the Laplace transform [11] as

$$V(u, v) = -\frac{1}{\kappa} \int_0^{+\infty} \frac{dq}{\sqrt{1 + \alpha^2 q^2}} e^{-q(u^2 + v^2)} (u^2 + v^2), \quad (\text{S-27})$$

where the dimensionless parameter $\alpha = r_0 / \kappa a_0^*$ is used instead of the screening length r_0 . In equations (S-26) and (S-27), we have used the formulas

$$r = u^2 + v^2, \quad \hat{l}_z = -\frac{i}{2} \left(v \frac{\partial}{\partial u} - u \frac{\partial}{\partial v} \right) \quad (\text{S-28})$$

obtained by the Levi-Civita transformation (S-25) for distance r and angular momentum \hat{l}_z .

Equation (S-26) is similar to those describing a two-dimensional anharmonic oscillator, suggesting we use the harmonic oscillator wave functions as a basis set and calculate necessary matrix elements by the algebraic approach based on annihilation and creation operators, well-known as the Feranchuk-Komarov operator method in Refs. [12, 13]. The first step is to rewrite the equation in the presentation of annihilation and creation operators, defined as

$$\hat{a} = \frac{1}{\sqrt{2}} (\hat{\alpha} - i\hat{\beta}), \quad \hat{a}^+ = \frac{1}{\sqrt{2}} (\hat{\alpha}^+ + i\hat{\beta}^+), \quad \hat{b} = \frac{1}{\sqrt{2}} (\hat{\alpha} + i\hat{\beta}), \quad \hat{b}^+ = \frac{1}{\sqrt{2}} (\hat{\alpha}^+ - i\hat{\beta}^+), \quad (\text{S-29})$$

where

$$\begin{aligned} \hat{\alpha} &= \sqrt{\frac{\omega}{2}} \left(u + \frac{1}{\omega} \frac{\partial}{\partial u} \right), & \hat{\alpha}^+ &= \sqrt{\frac{\omega}{2}} \left(u - \frac{1}{\omega} \frac{\partial}{\partial u} \right), \\ \hat{\beta} &= \sqrt{\frac{\omega}{2}} \left(v + \frac{1}{\omega} \frac{\partial}{\partial v} \right), & \hat{\beta}^+ &= \sqrt{\frac{\omega}{2}} \left(v - \frac{1}{\omega} \frac{\partial}{\partial v} \right). \end{aligned} \quad (\text{S-30})$$

Here, ω is a free parameter that manipulates the convergence rate of numerical calculations and does not affect the final energy spectrum. This parameter has been introduced and discussed in many references such as [12, 13] and references therein. These operators must obey the following commutation relations

$$[\hat{a}, \hat{a}^+] = [\hat{b}, \hat{b}^+] = 1, \quad [\hat{a}, \hat{a}] = [\hat{a}^+, \hat{a}^+] = [\hat{b}, \hat{b}] = [\hat{b}^+, \hat{b}^+] = 0, \quad (\text{S-31})$$

typical for annihilation and creation operators.

All the operators of Eq. (S-26) can be presented in terms of creation and annihilation operators as

$$\begin{aligned} - \left(\frac{\partial^2}{\partial u^2} + \frac{\partial^2}{\partial v^2} \right) &= \omega \left(-\hat{a}\hat{b} - \hat{a}^+\hat{b}^+ + \hat{a}^+\hat{a} + \hat{b}^+\hat{b} + 1 \right) \equiv \omega \hat{T}, \\ \hat{l}_z &= \frac{1}{2} (\hat{a}^+\hat{a} - \hat{b}^+\hat{b}), \\ u^2 + v^2 &= \frac{1}{\omega} (\hat{a}\hat{b} + \hat{a}^+\hat{b}^+ + \hat{a}^+\hat{a} + \hat{b}^+\hat{b} + 1), \\ u^4 - v^4 &= (\hat{a}^+\hat{a}^+ + \hat{b}^+\hat{b}^+ + \hat{a}\hat{a} + \hat{b}\hat{b} + 2\hat{b}^+\hat{a} + 2\hat{a}^+\hat{b}) (\hat{a}\hat{b} + \hat{a}^+\hat{b}^+ + \hat{a}^+\hat{a} + \hat{b}^+\hat{b} + 1). \end{aligned} \quad (\text{S-32})$$

Therefore, Eq. (S-26) is expressed as a secular equation

$$\hat{H} |\psi\rangle - E \hat{R} |\psi\rangle = 0, \quad (\text{S-33})$$

in which the explicit expressions of \hat{H} and \hat{R} are given as

$$\hat{R} = \hat{a}^+\hat{a} + \hat{b}^+\hat{b} + 1 + \hat{a}\hat{b} + \hat{a}^+\hat{b}^+, \quad (\text{S-34})$$

$$\hat{H} = \frac{\omega^2}{8} \hat{T} + \frac{1 - \sigma \gamma}{1 + \sigma} \frac{\gamma}{2} \hat{R} \hat{l}_z + \frac{\gamma^2}{8\omega^2} \hat{R}^3 - \omega \hat{V} + \frac{\sqrt{2\sigma\theta}}{1 + \sigma} \frac{\gamma}{2\omega} \hat{V}_{mS}. \quad (\text{S-35})$$

In Eq. (S-34), operator \hat{V} describes the Rytova-Keldysh interaction in the creation-annihilation-operator formalism and is written as the following integral

$$\hat{V} = -\frac{1}{\kappa} \int_0^\infty \frac{dq}{\sqrt{1 + \alpha^2 \omega^2 q^2}} e^{-q\hat{R}} \hat{R}, \quad (\text{S-36})$$

while operator

$$\hat{V}_{mS} = (\hat{a}^+\hat{a}^+ + \hat{b}^+\hat{b}^+ + \hat{a}\hat{a} + \hat{b}\hat{b} + 2\hat{b}^+\hat{a} + 2\hat{a}^+\hat{b}) (\hat{a}^+\hat{a} + \hat{b}^+\hat{b} + 1 + \hat{a}\hat{b} + \hat{a}^+\hat{b}^+) \quad (\text{S-37})$$

is of the thermo-induced motional Stark potential.

B. Matrix elements

The basis set in this method is chosen by the wave functions of the two-dimensional harmonic oscillator as

$$|k, m, \omega\rangle = \frac{1}{\sqrt{(k+m)!(k-m)!}} (\hat{a}^+)^{k+m} (\hat{b}^+)^{k-m} |0(\omega)\rangle, \quad (\text{S-38})$$

with the running numbers $k = |m|, |m|+1, |m|+2, \dots$ and $m = 0, \pm 1, \pm 2, \dots$. We note that the frequency ω can be regarded as a free parameter and will choose its value appropriate for regulating the convergence rate of the numerical solutions. Expanding the quantum wave function by this basis set as

$$|\psi^{(s)}(\omega)\rangle = \sum_{k=0}^s \sum_{m=0}^k C_{km}^{(s)} |k, m, \omega\rangle \quad (\text{S-39})$$

with $N = (s+1)(s+2)/2$ unknown coefficients $C_{km}^{(s)}$ needed to define and then putting these coefficients $C_{km}^{(s)}$ as a column matrix \mathbb{C} , Eq. (S-33) turns into a usual form of a generalized secular equation of the eigenproblem of an $N \times N$ -matrix \mathbb{H} with respect to \mathbb{R} as

$$(\mathbb{H} - E \mathbb{R}) \mathbb{C} = 0. \quad (\text{S-40})$$

The matrix eigenvalue equation can be solved using subroutine dsygvx.f of the Linear Algebra Package (LAPACK) [14]. Here, it is noticed that Schrödinger equation (2) is invariant under the transformation $x \rightarrow -x$, $\mathbf{B} \rightarrow -\mathbf{B}$; therefore, we can use only $m \geq 0$ in the expansion (S-39). In the wave function (S-39), we use only $(s+1)/(s+2)/2$ basis set functions so that the number s can be regarded as an approximation order of the solutions. In practice, we will increment the (s) -order until getting the desired precision.

Now, the second step of the Feranchuk Komarov operator method is to calculate elements of the matrices \mathbb{H} and \mathbb{R} . By algebraic calculations using the commutation relations (S-31), we find out the following useful matrix elements

$$\begin{aligned} N_{k,m}^{k',m'} &= \langle k', m', \omega | (\hat{a}^+ \hat{a} + \hat{b}^+ \hat{b}) | k, m, \omega \rangle = 2k \delta_{k',k} \delta_{m',m}, \\ M_{k,m}^{k',m'} &= \langle k', m', \omega | \hat{a}^+ \hat{b}^+ | k, m, \omega \rangle = \sqrt{(k+1)^2 - m^2} \delta_{k',k+1} \delta_{m',m}, \\ M_{k,m}^{k',m'} &= \langle k', m', \omega | \hat{a} \hat{b} | k, m, \omega \rangle = \sqrt{k^2 - m^2} \delta_{k',k-1} \delta_{m',m}, \end{aligned} \quad (\text{S-41})$$

which help us to determine matrix elements as

$$\mathcal{R}_{k,m}^{k',m'} = \langle k', m', \omega | \hat{R} | k, m, \omega \rangle = N_{k,m}^{k',m'} + M_{k,m}^{k',m'} + M_{k,m}^{k',m'+}, \quad (\text{S-42})$$

$$\begin{aligned} \mathcal{H}_{k,m}^{k',m'} &= \langle k', m', \omega | \hat{H} | k, m, \omega \rangle = \mathcal{T}_{k,m}^{k',m'} + \frac{1-\sigma}{1+\sigma} \frac{\gamma m}{2} (\mathcal{R})_{k,m}^{k',m'} + \frac{\gamma^2}{8\omega^2} (\mathcal{R}^3)_{k,m}^{k',m'} \\ &\quad - \omega (\mathcal{V}_{RK})_{k,m}^{k',m'} + \frac{\sqrt{2\sigma\theta}}{1+\sigma} \frac{\gamma}{2\omega} (\mathcal{V}_{mS})_{k,m}^{k',m'}, \end{aligned} \quad (\text{S-43})$$

where

$$\mathcal{T}_{k,m}^{k',m'} = \langle k', m', \omega | \hat{T} | k, m, \omega \rangle = N_{k,m}^{k',m'} - M_{k,m}^{k',m'} - M_{k,m}^{k',m'+}, \quad (\text{S-44})$$

and

$$\begin{aligned}
(\mathcal{R}^3)_{k',m'}^{k,m} &= \langle k', m', \omega | \hat{R}^3 | k, m, \omega \rangle \\
&= 2(5k^2 + 5k + 3 - 3m^2)(2k + 1)\delta_{k'k}\delta_{m'm} \\
&\quad + 6(5k^2 - 5k + 3 - 3m^2)\sqrt{k^2 - m^2}\delta_{k',k-1}\delta_{m'm} \\
&\quad + 3(2k - 1)\sqrt{k^2 - m^2}\sqrt{(k-1)^2 - m^2}\delta_{k',k-2}\delta_{m'm} \\
&\quad + \sqrt{k^2 - m^2}\sqrt{(k-1)^2 - m^2}\sqrt{(k-2)^2 - m^2}\delta_{k',k-3}\delta_{m'm} \\
&\quad + 6(5k^2 + 5k + 3 - 3m^2)\sqrt{(k+1)^2 - m^2}\delta_{k',k+1}\delta_{m'm} \\
&\quad + 3(2k + 3)\sqrt{(k+1)^2 - m^2}\sqrt{(k+2)^2 - m^2}\delta_{k',k+2}\delta_{m'm} \\
&\quad + \sqrt{(k+1)^2 - m^2}\sqrt{(k+2)^2 - m^2}\sqrt{(k+3)^2 - m^2}\delta_{k',k+3}\delta_{m'm}.
\end{aligned} \tag{S-45}$$

The matrix elements of the Rytova-Keldysh potential are calculated as

$$\begin{aligned}
(\mathcal{V}_{RK})_{k',m'}^{k,m} &= \langle k', m', \omega | \hat{V} | k, m, \omega \rangle \\
&= \left[(2k + 1)U_{k'k} + \sqrt{k^2 - m^2}U_{k'k-1} + \sqrt{(k+1)^2 - m^2}U_{k',k+1} \right] \delta_{m',m},
\end{aligned} \tag{S-46}$$

where

$$\begin{aligned}
U_{j'j} &= -\frac{1}{\kappa\alpha} \sum_{s=|m|}^{\min(j,j')} \sum_{t=0}^{j'+j-2s} (-1)^{j'+j+t} \binom{j'+j-2s}{t} \\
&\quad \times \sqrt{\binom{j'+m}{s+m}} \sqrt{\binom{j'-m}{s-m}} \sqrt{\binom{j+m}{s+m}} \sqrt{\binom{j-m}{s-m}} \\
&\quad \times \int_0^{+\infty} \frac{dq}{(1+q)^{2s+t+1} \sqrt{q^2 + 1/\omega^2\alpha^2}}.
\end{aligned} \tag{S-47}$$

The matrix elements associated with the thermo-induced motional Stark effect are calculated as

$$\begin{aligned}
(\mathcal{V}_{mS})_{k',m'}^{k,m} &= \langle k', m', \omega | \hat{V}_{mS} | k, m, \omega \rangle \\
&= \sqrt{(k+m)(k+m-1)(k+m-2)(k-m)}\delta_{k'+m',k+m-3}\delta_{k'-m',k-m-1} \\
&\quad + \sqrt{(k-m+3)(k-m+2)(k-m+1)(k+m+1)}\delta_{k'+m',k+m+1}\delta_{k'-m',k-m+3} \\
&\quad + \sqrt{(k+m+3)(k+m+2)(k+m+1)(k-m+1)}\delta_{k'+m',k+m+3}\delta_{k'-m',k-m+1} \\
&\quad + \sqrt{(k-m)(k-m-1)(k-m-2)(k+m)}\delta_{k'+m',k+m-1}\delta_{k'-m',k-m-2} \\
&\quad + \sqrt{(k+m+1)(k+m+2)(4k-2m+3)}\delta_{k'+m',k+m+2}\delta_{k'-m',k-m} \\
&\quad + 3\sqrt{(k-m)(k+m+1)(2k+1)}\delta_{k'+m',k+m+1}\delta_{k'-m',k-m-1} \\
&\quad + \sqrt{(k+m)(k+m-1)(2k-2m+1)}\delta_{k'+m',k+m-2}\delta_{k'-m',k-m} \\
&\quad + \sqrt{(k-m)(k-m-1)(4k+2m+1)}\delta_{k'+m',k+m}\delta_{k'-m',k-m-2} \\
&\quad + \sqrt{(k-m+1)(k-m+2)(4k+2m+3)}\delta_{k'+m',k+m}\delta_{k'-m',k-m+2} \\
&\quad + 3\sqrt{(k+m)(k-m+1)}\delta_{k'+m',k+m-1}\delta_{k'-m',k-m+1}.
\end{aligned} \tag{S-48}$$

C. Exciton energy spectrum for magnetoexciton in WSe₂ monolayer at zero and room temperatures

The third step is to solve Eq. (S-33) with all the matrix elements calculated. The free parameter ω is chosen to make the convergence rate suitable for our computing resources and the required precision of 8 decimal places. This matrix

eigenvalue equation can be solved by subroutine dsygvx.f of the Linear Algebra Package (LAPACK). We present here energies of magnetoexciton in monolayer WSe₂ for $1s$, $2s$, $2p_{-1}$, $2p_{+1}$, and $3s$ states with magnetic intensity up to 500 Tesla. In the paper, we show fewer results for magnetic intensities, up to 90 Tesla produced in laboratories. We note that the method is applicable for the case with no magnetic field by dropping the thermo-induced term.

TABLE S-II. Energies of $1s$ states (meV) with different magnetic intensity B (Tesla) at temperature 0 K and 300 K for $r_0 = 4.2086$ nm, $\mu = 0.2039 m_e$, $\kappa = 4.5$.

B (T)	0 K	300 K	B (T)	0 K	300 K	B (T)	0 K	300 K
0	-168.552041	-168.552041	8	-168.533899	-168.535348	160	-161.809395	-162.242261
0.1	-168.552037	-168.552039	9	-168.529081	-168.530915	170	-160.998758	-161.473738
0.2	-168.552030	-168.552032	10	-168.523698	-168.525961	180	-160.150516	-160.667960
0.3	-168.552015	-168.552019	20	-168.438787	-168.447803	190	-159.265944	-159.826064
0.4	-168.551995	-168.552000	30	-168.297672	-168.317802	200	-158.346277	-158.949161
0.5	-168.551969	-168.551977	40	-168.100937	-168.136347	220	-156.406369	-157.094633
0.6	-168.551938	-168.551948	50	-167.849370	-167.903971	240	-154.339764	-155.112661
0.7	-168.551901	-168.551913	60	-167.543935	-167.621338	260	-152.154735	-153.011013
0.8	-168.551859	-168.551874	70	-167.185740	-167.289235	280	-149.858881	-150.796930
0.9	-168.551809	-168.551830	80	-166.776017	-166.908547	300	-147.459176	-148.477134
1	-168.551757	-168.551780	90	-166.316080	-166.480251	320	-144.962011	-146.057853
2	-168.550907	-168.550998	100	-165.807310	-166.005392	340	-142.373248	-143.544846
3	-168.549489	-168.549693	110	-165.251129	-165.485072	360	-139.698262	-140.943439
4	-168.547504	-168.547868	120	-164.648977	-164.920434	380	-136.941989	-138.258552
5	-168.544953	-168.545520	130	-164.002303	-164.312647	400	-134.108968	-135.494735
6	-168.541835	-168.542651	140	-163.312539	-163.662897	500	-118.928095	-120.628607

TABLE S-III. Energies of $2s$ states (meV) with different magnetic intensity B (Tesla) at temperature 0 K and 300 K for $r_0 = 4.2086$ nm, $\mu = 0.2039 m_e$, $\kappa = 4.5$.

B (T)	0 K	300 K	B (T)	0 K	300 K	B (T)	0 K	300 K
0	-38.553893	-38.553893	8	-38.240316	-38.199502	160	25.940847	27.459482
0.1	-38.553843	-38.553837	9	-38.157907	-38.106499	170	31.831398	33.306752
0.2	-38.553695	-38.553669	10	-38.066222	-38.003093	180	37.819418	39.245494
0.3	-38.553448	-38.553390	20	-36.669754	-36.436785	190	43.897110	45.269125
0.4	-38.553102	-38.552998	30	-34.506863	-34.043385	200	50.057588	51.371775
0.5	-38.552657	-38.552495	40	-31.719080	-31.011684	220	62.603138	63.793606
0.6	-38.552114	-38.551880	50	-28.421034	-27.487797	240	75.414636	76.474757
0.7	-38.551471	-38.551153	60	-24.700889	-23.574784	260	88.458650	89.385396
0.8	-38.550730	-38.550314	70	-20.626315	-19.344546	280	101.707813	102.500637
0.9	-38.549890	-38.549364	80	-16.249938	-14.848486	300	115.139432	115.799484
1	-38.548951	-38.548302	90	-11.613374	-10.124672	320	128.734481	129.264053
2	-38.534134	-38.531539	100	-6.750083	-5.202292	340	142.476846	142.878985
3	-38.509466	-38.503636	110	-1.687376	-0.104429	360	156.352755	156.630985
4	-38.474989	-38.464645	120	3.552157	5.150194	380	170.350347	170.508473
5	-38.430758	-38.414637	130	8.949610	10.546065	400	184.459323	184.501297
6	-38.376843	-38.353703	140	14.488990	16.070108	500	256.394876	255.914993

TABLE S-IV. Energies of $2p_{-1}$ states (meV) with different magnetic intensity B (Tesla) at temperature 0 K and 300 K for $r_0 = 4.2086$ nm, $\mu = 0.2039 m_e$, $\kappa = 4.5$.

B (T)	0 K	300 K	B (T)	0 K	300 K	B (T)	0 K	300 K
0	-49.781570	-49.781570	8	-49.695186	-49.807901	160	-14.823995	-20.622206
0.1	-49.782364	-49.782378	9	-49.663271	-49.807384	170	-11.440536	-17.322395
0.2	-49.783110	-49.783167	10	-49.626753	-49.805961	180	-7.987731	-13.938192
0.3	-49.783809	-49.783937	20	-49.017308	-49.709812	190	-4.470652	-10.476915
0.4	-49.784460	-49.784689	30	-47.998661	-49.363442	200	-0.893804	-6.944978
0.5	-49.785063	-49.785423	40	-46.624801	-48.677958	220	6.423547	0.308947
0.6	-49.785619	-49.786139	50	-44.946648	-47.636100	240	13.936854	7.785739
0.7	-49.786127	-49.786838	60	-43.007928	-46.258786	260	21.623704	15.455403
0.8	-49.786587	-49.787521	70	-40.844855	-44.580043	280	29.465547	23.293827
0.9	-49.787000	-49.788186	80	-38.487089	-42.635354	300	37.446831	31.281380
1	-49.787365	-49.788835	90	-35.958943	-40.457323	320	45.554375	39.401882
2	-49.788396	-49.794511	100	-33.280459	-38.074472	340	53.776897	47.641857
3	-49.784671	-49.798912	110	-30.468298	-35.511273	360	62.104653	55.989959
4	-49.776198	-49.802285	120	-27.536427	-32.788581	380	70.529166	64.436547
5	-49.762993	-49.804804	130	-24.496664	-29.924152	400	79.043007	72.973350
6	-49.745074	-49.806567	140	-21.359086	-26.933141	500	122.746523	116.789306

TABLE S-V. Energies of $2p_{+1}$ states (meV) with different magnetic intensity B (Tesla) at temperature 0 K and 300 K for $r_0 = 4.2086$ nm, $\mu = 0.2039 m_e$, $\kappa = 4.5$.

B (T)	0 K	300 K	B (T)	0 K	300 K	B (T)	0 K	300 K
0	-49.781570	-49.781570	8	-49.564342	-49.627092	160	-12.207129	-15.179979
0.1	-49.780728	-49.780743	9	-49.516073	-49.592434	170	-8.660116	-11.759609
0.2	-49.779839	-49.779895	10	-49.463199	-49.554019	180	-5.043756	-8.263017
0.3	-49.778902	-49.779027	20	-48.690200	-48.961283	190	-1.363123	-4.695704
0.4	-49.777917	-49.778139	30	-47.507998	-48.000679	200	2.377279	-1.062559
0.5	-49.776885	-49.777231	40	-45.970585	-46.702090	220	10.021739	6.384172
0.6	-49.775806	-49.776300	50	-44.128877	-45.101426	240	17.862153	14.047174
0.7	-49.774678	-49.775347	60	-42.026603	-43.234227	260	25.876112	21.901854
0.8	-49.773503	-49.774373	70	-39.699976	-41.132761	280	34.045063	29.927753
0.9	-49.772280	-49.773376	80	-37.178656	-38.825110	300	42.353455	38.107629
1	-49.771009	-49.772357	90	-34.486955	-36.335246	320	50.788108	46.426794
2	-49.755685	-49.760828	100	-31.644917	-33.683487	340	59.337737	54.872614
3	-49.735604	-49.746637	110	-28.669202	-30.887043	360	67.992602	63.434133
4	-49.710777	-49.729480	120	-25.573778	-27.960544	380	76.744223	72.101781
5	-49.681216	-49.709113	130	-22.370460	-24.916482	400	85.585173	80.867150
6	-49.646942	-49.685347	140	-19.069329	-21.765588	500	130.924230	125.926405

TABLE S-VI. Energies of $3s$ states (meV) with different magnetic intensity B (Tesla) at temperature 0 K and 300 K for $r_0 = 4.2086$ nm, $\mu = 0.2039 m_e$, $\kappa = 4.5$.

B (T)	0 K	300 K	B (T)	0 K	300 K	B (T)	0 K	300 K
0	-16.551620	-16.551620	8	-15.001325	-13.427883	160	137.144400	140.552814
0.1	-16.551360	-16.551008	9	-14.619501	-12.803618	170	149.056334	152.353631
0.2	-16.550579	-16.549174	10	-14.204125	-12.148735	180	161.055614	164.238685
0.3	-16.549277	-16.546120	20	-8.618289	-5.574895	190	173.134690	176.201768
0.4	-16.547456	-16.541853	30	-1.282591	2.143361	200	185.286995	188.237342
0.5	-16.545114	-16.536377	40	7.125278	10.705982	220	209.788965	212.506621
0.6	-16.542253	-16.529703	50	16.266355	19.925459	240	234.523093	237.012433
0.7	-16.538873	-16.521841	60	25.946909	29.681931	260	259.458929	261.726817
0.8	-16.534974	-16.512804	70	36.044740	39.855984	280	284.571899	286.626551
0.9	-16.530558	-16.502206	80	46.477076	50.343774	300	309.841859	311.692133
1	-16.525624	-16.489263	90	57.184816	61.074853	320	335.252069	336.907025
2	-16.448058	-16.271898	100	68.124039	72.004863	340	360.788456	362.257080
3	-16.320131	-15.948198	110	79.261069	83.104559	360	386.439062	387.730100
4	-16.143689	-15.545495	120	90.569426	94.353023	380	412.193633	413.315496
5	-15.921016	-15.076549	130	102.027862	105.734178	400	438.043305	439.004012
6	-15.654647	-14.570256	140	113.619029	117.235016	500	568.478171	568.738960

S-VIII. ANALYSIS OF THERMO-INDUCED EFFECT BY THE PERTURBATION METHOD

In the center-of-mass frame of reference, the relative motion between the electron and hole in neutral exciton is described by the partial wave function $\psi_{\mathbf{K}}(\mathbf{r})$ corresponding to the pseudomomentum \mathbf{K} . This wavefunction is governed by the following one-particle Schrödinger equation

$$\left\{ \frac{\hat{\mathbf{p}}^2}{2\mu} + V_{RK}(\mathbf{r}) + V_{Zeeman}(\mathbf{r}) + V_{diamag}(\mathbf{r}) + V_{mS}(\mathbf{r}) - E \right\} \psi_{\mathbf{K}}(\mathbf{r}) = 0. \quad (\text{S-49})$$

Here, we use the Rytova-Keldysh potential

$$V_{RK}(\mathbf{r}) = -\frac{e^2}{8\epsilon_0 r_0} \left[H_0\left(\frac{\kappa r}{r_0}\right) - Y_0\left(\frac{\kappa r}{r_0}\right) \right] \quad (\text{S-50})$$

to describe the electron-hole interaction as in many Refs. [15–20]. The next two terms are the Zeeman-splitting and diamagnetic potentials, respectively,

$$V_{Zeeman}(\mathbf{r}) = \frac{1 - \sigma}{1 + \sigma} \frac{eB}{2\mu} \hat{l}_z, \quad V_{diamag}(\mathbf{r}) = \frac{e^2 B^2}{8\mu} \mathbf{r}^2, \quad (\text{S-51})$$

while the last term is the thermo-induced motional Stark potential

$$V_{mS}(\mathbf{r}) = -\sqrt{\frac{2k_B T}{M}} eB r \cos \varphi. \quad (\text{S-52})$$

For illustration, we show the effective potential of equation (S-49) in Fig. S-1 for two cases, with and without the thermo-induced motional Stark potential, i.e., $T \neq 0$ and $T = 0$. This figure clearly shows that at room temperature, the contribution of the added term on the effective potential is noticeable for the $2s$ and higher Rydberg states, and it would influence the exciton energy spectra.

The effective potential in Fig. S-1 shows no tunneling effect, even considering the thermo-induced motional Stark potential. That means the exciton is always in its bound states, unlike the well-known LoSurdo-Stark effect in the two-dimensional electron gas [21, 22]. Indeed, this fact can be understood from the thermo-induced motional Stark potential (S-52). This part is linearly proportional to the variable x ; however, the main part of the effective potential, the diamagnetic potential $V_{diamag}(\mathbf{r})$, is quadratic proportional to the electron-hole distance and consequently dominant at the large separation of the electron-hole pair that keeps the exciton in bound states. Instead of tunneling, we believe the thermo-induced motional Stark potential cause the Stark shift in the energy spectra, as observed in numerical calculations in Subsection S-VII C.

Now we analyze energy spectra of neutral exciton in monolayer TMDC monolayer, solving the Schrödinger equation (S-49) in the low and high limits of magnetic field intensity by the perturbation theory.

A. In low magnetic field intensity limit

The Schrödinger equation (S-49) without a magnetic field ($B = 0$) is much simpler as

$$\left\{ \frac{\hat{\mathbf{p}}^2}{2\mu} + V_{RK}(\mathbf{r}) - E^{(0)} \right\} \psi^{(0)}(\mathbf{r}) = 0 \quad (\text{S-53})$$

because there are no Zeeman-splitting, diamagnetic, and even thermo-induced motional Stark potentials. Consequently, the energy spectrum and eigenstate of neutral exciton are found as $E_{nm}^{(0)}$ and $\psi_{nm}^{(0)}(\mathbf{r}) = R_{nm}^{(0)}(r) \frac{e^{im\varphi}}{\sqrt{2\pi}}$, respectively. Here, m is the magnetic quantum number associated with the angular momentum \hat{l}_z ; and $n = n_r + |m| + 1$ is defined as the principal quantum number, with n_r being the node number of the radial wavefunction $R_{nm}^{(0)}(r)$. At the state $|nm\rangle$, the average separation between electron and hole is $\langle r \rangle_{nm} = \langle R_{nm}^{(0)} | r | R_{nm}^{(0)} \rangle$. We note that $E_{nm}^{(0)}$ and $R_{nm}^{(0)}(r)$ are obtained by numerical calculation, particularly by the method described in Sec. S-VII.

Turning on the magnetic field ($B > 0$) such that its typical length is much larger than the average exciton radius, $l_B = \sqrt{\frac{\hbar}{eB}} \gg \langle r \rangle_{nm}$, all the Zeeman-splitting, diamagnetic, and thermo-induced motional Stark potentials can be treated as perturbed interactions besides the zeroth-order Hamiltonian in Eq. (S-53). Both the Zeeman-splitting and diamagnetic potentials contribute to the first-order correction via Zeeman-splitting and diamagnetic energies

$$\langle \psi_{nm}^{(0)} | V_{Zeeman} | \psi_{nm}^{(0)} \rangle = \frac{1 - \sigma}{1 + \sigma} \frac{\hbar m}{2\mu} eB, \quad (\text{S-54})$$

$$\langle \psi_{nm}^{(0)} | V_{diamag} | \psi_{nm}^{(0)} \rangle = \frac{e^2 B^2}{8\mu} \langle r^2 \rangle_{nm}. \quad (\text{S-55})$$

Since the original state $\psi_{nm}^{(0)}(\mathbf{r})$ exhibits the $SO(2)$ symmetry of neutral exciton and the thermo-induced motional Stark potential $V_{mS}(\mathbf{r})$ is proportional to $r \cos \varphi$, its first-order correction must vanish

$$\langle \psi_{nm}^{(0)} | V_{mS} | \psi_{nm}^{(0)} \rangle = 0. \quad (\text{S-56})$$

However, the thermo-induced motional Stark effect solely appears in the second-order correction of energy as

$$\sum_{(n'm') \neq (nm)} \frac{|\langle \psi_{nm}^{(0)} | V_{mS} | \psi_{n'm'}^{(0)} \rangle|^2}{E_{nm}^{(0)} - E_{n'm'}^{(0)}} = -\alpha_{nm} \frac{k_B T}{M} e^2 B^2. \quad (\text{S-57})$$

Here, α_{nm} is the zero-field polarizability of the exciton

$$\alpha_{nm} = - \sum_{\substack{n' \geq |m'| + 1 \\ m' = m \pm 1}} \frac{\left| \int_0^{+\infty} R_{nm}^{(0)*}(r) R_{n'm'}^{(0)}(r) r^2 dr \right|^2}{E_{nm}^{(0)} - E_{n'm'}^{(0)}}. \quad (\text{S-58})$$

Finally, the energy of magnetoexciton at the state $|nm\rangle$ is obtained as

$$E_{nm}^{(2)}(B, T) \approx E_{nm}^{(0)} + \frac{1 - \sigma}{1 + \sigma} \frac{\hbar m}{2\mu} eB + \frac{e^2 B^2}{8\mu} \langle r^2 \rangle_{nm} - \alpha_{nm} \frac{k_B T}{M} e^2 B^2. \quad (\text{S-59})$$

This is the equation (4) in the main text. In other words, the quadratic thermo-induced motional Stark correction in the low magnetic field is proportional to the square of magnetic field strength

$$\Delta E_{nm}(B, T) = E_{nm}^{(2)}(B, T) - E_{nm}(B, 0) \approx \alpha_{nm} \frac{k_B T}{M} e^2 B^2. \quad (\text{S-60})$$

From energies of the states $1s$, $2s$, $3s$, $2p_{-1}$, and $2p_{+1}$ in Tables S-II, S-III, S-IV, S-V, and S-VI, the quadratic thermo-induced motional Stark corrections in the low magnetic field $\Delta E_{nm}(B, T)$ for these states are numerically determined. Consequently, the zero-field polarizability of exciton α_{nm} and the thermo-induced Stark correction on diamagnetic coefficient $\Delta\sigma_{nm} = -\frac{e^2}{M} \alpha_{nm} k_B T$ are revealed by fitting the data of $\Delta E_{nm}(B, T)$ versus B^2 in Eq. (S-60). These results are presented in Table 2 of the main text.

Figure S-2 indicates that the quadratic thermo-induced motional Stark corrections of $1s$, $2s$, $3s$, $2p_{-1}$, and $2p_{+1}$ states depend on B^2 for the low magnetic field regime.

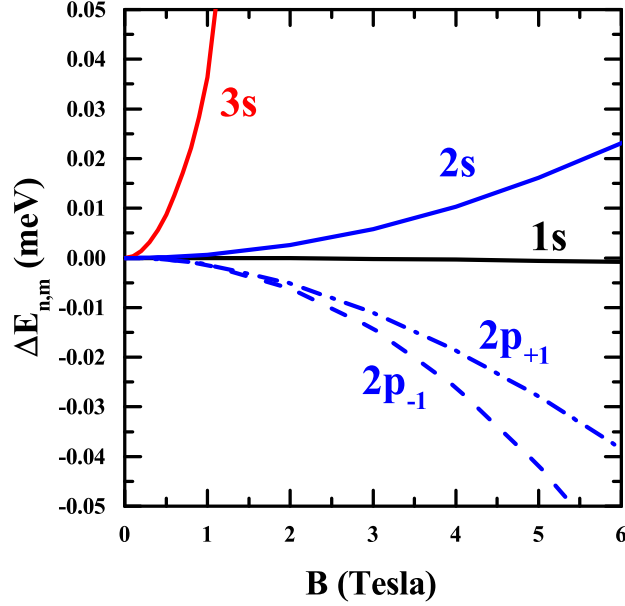


FIG. S-2. The dependence of quadratic thermo-induced motional Stark corrections $\Delta E_{nm}(B, T)$ for various states: $1s$ (black), $2s$ (red), $3s$ (blue), $2p_{-1}$ (blue dashed), and $2p_{+1}$ (blue dot-dashed) on magnetic field strength B for the low magnetic field regime.

B. In high magnetic field intensity limit

Suppose the magnetic field is so large that its typical length is much smaller than the average exciton radius, $l_B \ll \langle r \rangle_{nm}^{(0)}$; the diamagnetic potential $V_{diamag} = \frac{e^2 B^2}{8\mu} \mathbf{r}^2$ (the harmonic oscillator potential of frequency $\omega_B = eB/2\mu$) becomes dominant. In this case, the energy spectrum tends to the conventional Landau levels. Within the effect of Zeeman-splitting potential V_{Zeeman} , these zero-temperature Landau levels are shifted as

$$E_{nm}^{(0)}(B \rightarrow \infty, T = 0) = \frac{\hbar}{2\mu} \left(2n - |m| - 1 + \frac{1 - \sigma}{1 + \sigma} m \right) eB, \quad (\text{S-61})$$

and the corresponding eigenstate is of the isotropic harmonic oscillator with the wave function

$$\psi_{nm}^{(0)}(\mathbf{r}) = \frac{1}{l_B} R_{nm}^{(0)} \left(\frac{r^2}{l_B^2} \right) \frac{e^{im\varphi}}{\sqrt{2\pi}}, \quad (\text{S-62})$$

where $R_{nm}^{(0)}$ is the dimensionless radial wave function of the dimensionless variable r^2/l_B^2 .

Similar to the low magnetic field limit in the finite temperature, the thermo-induced motional Stark potential in the high magnetic field limit contributes to the second-order correction in the perturbation theory as

$$\sum_{(n', m') \neq (n, m)} \frac{\left| \langle \psi_{nm}^{(0)} | V_{mS} | \psi_{n'm'}^{(0)} \rangle \right|^2}{E_{nm}^{(0)} - E_{n'm'}^{(0)}}. \quad (\text{S-63})$$

It results in the energy spectrum of magnetoexciton behaving as

$$E_{nm}^{(2)}(B, T) \approx \frac{\hbar}{2\mu} \left(2n - |m| - 1 + \frac{1 - \sigma}{1 + \sigma} m \right) eB - \frac{8\mu\beta_{nm}}{M} k_B T, \quad (\text{S-64})$$

where β_{nm} is a dimensionless constant calculated as

$$\begin{aligned} \beta_{nm} &= -\frac{e^2 B^2}{4\mu} \sum_{(n',m') \neq (n,m)} \frac{\left| \langle \psi_{nm}^{(0)} | r \cos \varphi | \psi_{n'm'}^{(0)} \rangle \right|^2}{E_{nm}^{(0)} - E_{n'm'}^{(0)}} \\ &= - \sum_{\substack{n' \geq |m'|+1 \\ m' = m \pm 1}} \frac{\frac{1}{4} \left| \int_0^{+\infty} R_{nm}^{(0)*}(x) R_{n'm'}^{(0)}(x) \sqrt{x} dx \right|^2}{2(n-n') - (|m| - |m'|) + \frac{1-\sigma}{1+\sigma}(m-m')}. \end{aligned} \quad (\text{S-65})$$

Therefore, the quadratic thermo-induced motional Stark correction in the high magnetic field limit solely depends on temperature as

$$\Delta E_{nm}(B, T) = E_{nm}^{(2)}(B, T) - E_{nm}(B, 0) \approx -\frac{8\mu\beta_{nm}}{M} k_B T. \quad (\text{S-66})$$

Although these calculations are only valid for extremely high magnetic intensity, the magnetic independence of $\Delta E_{nm}(B, T)$ can still be observed in our numerical calculations. Figure S-3 below illustrates how the quadratic thermo-induced motional Stark correction $\Delta E_{nm}(B, T)$ constantly behaves in the high magnetic field regime.

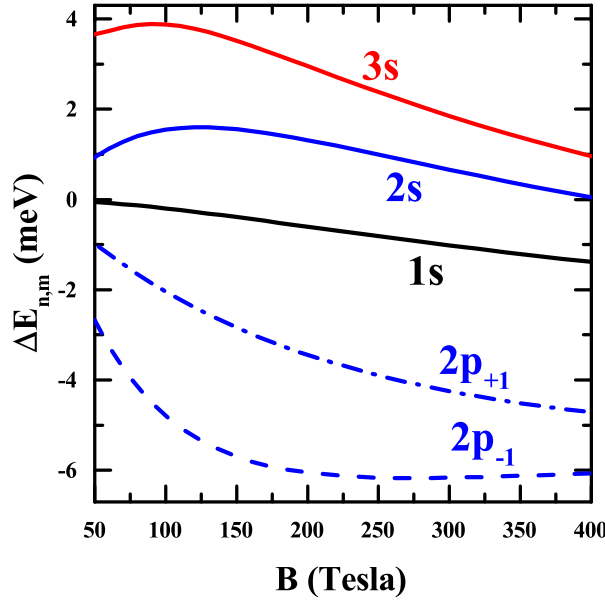


FIG. S-3. The dependence of quadratic thermo-induced motional Stark correction $\Delta E_{nm}(B, T)$ for various states: 1s (black), 2s (red), 3s (blue), $2p_{-1}$ (blue dashed), and $2p_{+1}$ (blue dot-dashed) on magnetic field strength B for the high magnetic field regime.

C. Thermo-induced deformation of magnetoexciton wave functions by symmetry-breaking mechanism

The influence of thermo-induced motional Stark potential on the wave function of magnetoexciton is also important because this potential breaks the $SO(2)$ symmetry of magnetoexciton. Indeed, the angular momentum \hat{l}_z is no longer conserved when we turn on the thermo-induced motional Stark potential. Hence, we can witness the deformation of magnetoexciton's orbital from this breaking symmetry mechanism.

In detail, the relative Hamiltonian of electron-hole pair under the presence of the thermo-induced motional Stark potential reads

$$\hat{H}_{rel}(T) = \hat{H}_{rel}(0) + V_{mS}(\mathbf{r}), \quad (\text{S-67})$$

where the zero-temperature relative Hamiltonian is given as

$$\begin{aligned}\hat{H}_{rel}(0) &= \frac{1}{2\mu}\hat{\mathbf{p}}^2 + \frac{1-\sigma}{1+\sigma}\frac{eB}{2\mu}\hat{l}_z + \frac{e^2B^2}{8\mu}r^2 + V_{RK}(r) \\ &= -\frac{\hbar^2}{2\mu}\left[\frac{1}{r}\frac{\partial}{\partial r}\left(r\frac{\partial}{\partial r}\right)\right] + \frac{\hat{l}_z^2}{2\mu} + \frac{1-\sigma}{1+\sigma}\frac{eB}{2\mu}\hat{l}_z + \frac{e^2B^2}{8\mu}r^2 + V_{RK}(r).\end{aligned}\quad (\text{S-68})$$

One can easily verify that each term of the zero-temperature relative Hamiltonian (S-68) commutes with the relative angular momentum $\hat{l}_z = -i\hbar\partial/\partial\varphi$. The first, fourth, and fifth terms in Eq. (S-68) commute with \hat{l}_z because they only depend on the radial variable r and do not depend on the angle variable φ . On the other hand, the second and third terms are polynomials of \hat{l}_z by themselves and trivially commute with \hat{l}_z . Then

$$[\hat{l}_z, \hat{H}_{rel}(0)] = 0, \quad (\text{S-69})$$

i.e., the angular momentum \hat{l}_z is conserved at zero temperature $T = 0$. In other words, the magnetoexciton at zero temperature exhibits the $SO(2)$ symmetry. A direct consequence of this $SO(2)$ symmetry is that the wavefunction of the relative motion of magnetoexciton must be in the following form

$$\psi_{nm}^{(0)}(\mathbf{r}) = R_{nm}^{(0)}(r)\frac{e^{im\varphi}}{\sqrt{2\pi}}, \quad (\text{S-70})$$

where its modulus does not depend on the angle variable φ :

$$|\psi_{nm}^{(0)}(\mathbf{r})|^2 = |R_{nm}^{(0)}(r)|^2. \quad (\text{S-71})$$

We say that magnetoexciton at zero temperature has circular orbitals.

The scenario changes when we turn on the temperature $T \neq 0$. Including the thermo-induced motional Stark potential $V_{mS}(\mathbf{r}) = -\sqrt{\frac{2k_B T}{M}}eBr \cos\varphi$ makes the angular momentum \hat{l}_z no longer commutes with the Hamiltonian

$$\begin{aligned}[\hat{l}_z, \hat{H}_{rel}(T)] &= [\hat{l}_z, \hat{H}_{rel}(0)] + [\hat{l}_z, V_{mS}(\mathbf{r})] \\ &= \left[-i\hbar\frac{\partial}{\partial\varphi}, -\sqrt{\frac{2k_B T}{M}}eBr \cos\varphi\right] = -i\hbar\sqrt{\frac{2k_B T}{M}}eBr \sin\varphi \neq 0.\end{aligned}\quad (\text{S-72})$$

We say that the thermo-induced motional Stark potential breaks the $SO(2)$ symmetry of magnetoexciton. Therefore, it is expected that the thermo-induced motional Stark effect could deform the magnetoexciton's orbitals and change the average distance of the electron-hole pair. We consider the zero-temperature magnetoexciton as zeroth-order Hamiltonian and then treat the thermo-induced motional Stark potential as a perturbation term. The zeroth-order Schrödinger equation for magnetoexciton reads

$$\left\{\frac{\hat{\mathbf{p}}^2}{2\mu} + V_{RK}(\mathbf{r}) + V_{Zeeman}(\mathbf{r}) + V_{diamag}(\mathbf{r}) - E^{(0)}\right\}\psi_{\mathbf{K}}^{(0)}(\mathbf{r}) = 0. \quad (\text{S-73})$$

The energy spectrum and eigenstates of magnetoexciton are $E_{nm}^{(0)}$ and $\psi_{nm}^{(0)}(\mathbf{r}) = R_{nm}^{(0)}(r)\frac{e^{im\varphi}}{\sqrt{2\pi}}$, respectively.

Taking into account the first-order correction caused by this thermo-induced motional Stark potential, we obtain the temperature-dependent wave functions of magnetoexciton as

$$\begin{aligned}\psi_{nm}^T(\mathbf{r}) &\approx R_{nm}^{(0)}(r)\frac{e^{im\varphi}}{\sqrt{2\pi}} - \sqrt{\frac{2k_B T}{M}}eB \sum_{n' \geq |m+1|+1} f_{nm;n',m+1} R_{n',m+1}^{(0)}(r)\frac{e^{i(m+1)\varphi}}{\sqrt{2\pi}} \\ &\quad - \sqrt{\frac{2k_B T}{M}}eB \sum_{n' \geq |m-1|+1} f_{nm;n',m-1} R_{n',m-1}^{(0)}(r)\frac{e^{i(m-1)\varphi}}{\sqrt{2\pi}},\end{aligned}\quad (\text{S-74})$$

where the coefficients $f_{nm;n'm'}$ are given by the following integrals

$$f_{nm;n'm'} = \frac{\int_0^{+\infty} R_{nm}^{(0)*}(r)R_{n'm'}^{(0)}(r)r^2 dr}{E_{nm}^{(0)} - E_{n'm'}^{(0)}}. \quad (\text{S-75})$$

As a result, the orbital of magnetoexciton is deformed along the Ox axis because the probability density is no longer angle-independent

$$\begin{aligned}
|\psi_{nm}^T(\mathbf{r})|^2 &= \frac{1}{2\pi} \left| R_{nm}^{(0)}(r) \right|^2 - \frac{1}{2\pi} \sqrt{\frac{2k_B T}{M}} eB \sum_{n'} \left(f_{nm;n',m+1} R_{nm}^{(0)*}(r) R_{n',m+1}^{(0)}(r) e^{i\varphi} \right. \\
&\quad \left. + f_{nm;n',m-1} R_{nm}^{(0)*}(r) R_{n',m-1}^{(0)}(r) e^{-i\varphi} + c.c \right) \\
&\quad + \frac{1}{2\pi} \frac{2k_B T}{M} e^2 B^2 \sum_{n',n''} \left[f_{nm;n'',m+1}^* f_{nm;n',m+1} R_{n'',m+1}^{(0)*}(r) R_{n',m+1}^{(0)}(r) \right. \\
&\quad \left. + f_{nm;n'',m-1}^* f_{nm;n',m-1} R_{n'',m-1}^{(0)*}(r) R_{n',m-1}^{(0)}(r) \right. \\
&\quad \left. + \left(f_{nm;n'',m-1}^* f_{nm;n',m+1} R_{n'',m+1}^{(0)*}(r) R_{n',m-1}^{(0)}(r) e^{-2i\varphi} + c.c \right) \right]. \tag{S-76}
\end{aligned}$$

The symmetry breaking is clear in the squared modulus of the wave functions $|\psi|^2$ of $2s$, $3s$, $2p_{-1}$ and $2p_{+1}$ states at temperatures of 0K and 300K, as shown in Fig. S-4. The effect is also seen in the orbital of the $1s$ state but is very slight.

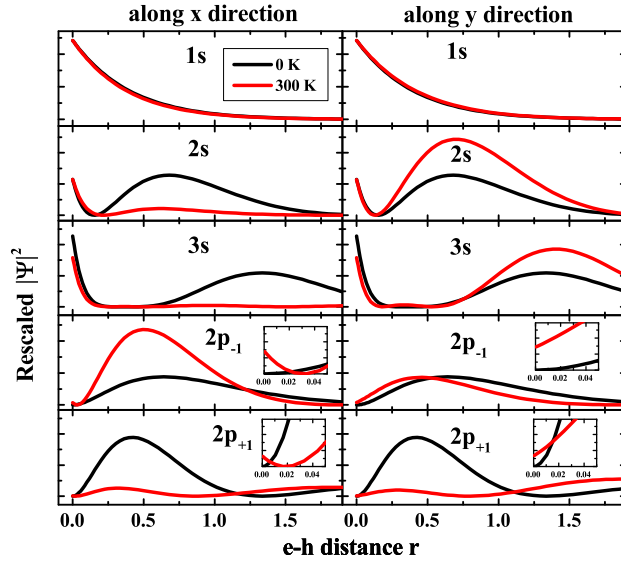


FIG. S-4. Squared modulus of wavefunction $|\Psi|^2$ as a function of electron-hole separation r along x and y axis for different states.

A direct consequence of the orbital's deformation is the change of the average separation between electron and hole in magnetoexcitons

$$\begin{aligned}
\langle r \rangle_{nm}^T &= \int_0^{+\infty} \int_0^{2\pi} |\psi_{nm}^T(\mathbf{r})|^2 r^2 dr d\varphi \\
&= \int_0^{+\infty} \left| R_{nm}^{(0)}(r) \right|^2 r^2 dr + \frac{2k_B T}{M} e^2 B^2 \sum_{\substack{n',n'' \\ m'=m\pm 1}} f_{nm;n''m'}^* f_{nm;n'm'} \int_0^{+\infty} R_{n''m'}^{(0)*}(r) R_{n'm'}^{(0)}(r) r^2 dr \\
&= \langle r \rangle_{nm} + \gamma_{nm} e^2 B^2 \frac{k_B T}{M}, \tag{S-77}
\end{aligned}$$

with

$$\gamma_{nm} = \sum_{\substack{n',n'' \geq |m'|+1 \\ m'=m\pm 1}} f_{nm;n''m'}^* f_{nm;n'm'} \int_0^{+\infty} R_{n''m'}^{(0)*}(r) R_{n'm'}^{(0)}(r) r^2 dr. \tag{S-78}$$

Figure S-5 shows how the average electron-hole separation $\langle r \rangle$ depends on the magnetic field at zero and room temperatures. As seen in the small panels, the change $\Delta \langle r \rangle$ is proportional to B^2 for the low magnetic field limit, as predicted by the perturbation theory.

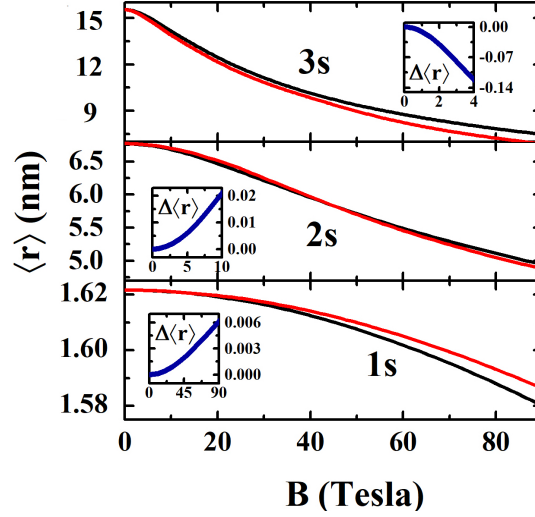


FIG. S-5. Magnetic field dependence of average radius $\langle r \rangle$ of magnetoexciton with different states. Small panels show the change of average radius $\Delta \langle r \rangle$ by temperature.

D. Squared modulus of magnetoexciton wave functions at zero separation of electron-hole pair for np and nd states

According to Elliot formula (see equation (9) in the main text), the signal of exciton peaks on the absorption spectra mainly depends on the oscillation strength, which is proportional to the squared modulus of the wave function $|\psi_{nm}(\mathbf{r} = 0)|^2$ at zero distance of the electron-hole pair.

At zero temperature $T = 0$, the conservation of the angular momentum \hat{l}_z , i. e., the $SO(2)$ symmetry of Schrödinger equation (S-73), suggests the form of the radial wave function as follows

$$R_{nm}^{(0)} \propto r^{|m|} e^{-f(r)} u(r). \quad (\text{S-79})$$

Therefore, except for the s -states, the wave function at zero distance $r = 0$ for all other states must vanish

$$\left| \psi_{np}^{(0)}(\mathbf{r} = 0) \right|^2 = \left| \psi_{nd}^{(0)}(\mathbf{r} = 0) \right|^2 = \dots = 0. \quad (\text{S-80})$$

When we turn on the temperature ($T \neq 0$), the orbital of magnetoexciton is deformed, as in Eq. (S-76) based on the perturbation theory calculations. Hence, for p -states, the squared modulus becomes non-vanished

$$\left| \psi_{np}^T(\mathbf{r} = 0) \right|^2 = \frac{2k_B T}{M} e^2 B^2 \sum_{n', n''} f_{np; n''s}^* f_{np; n's} \psi_{n''s}^{(0)*}(\mathbf{r} = 0) \psi_{n's}^{(0)}(\mathbf{r} = 0) \propto \frac{k_B T}{M}. \quad (\text{S-81})$$

Nonzero wavefunction at zero e-h separation is witnessed for $2p_{\pm 1}$ states as shown in small panels in Fig. S-4. This circumstance leads to the emergence of the p -state peaks on the absorption spectra of neutral magnetoexciton, as shown in Fig. 4 of the main text and more details in Fig. S-6.

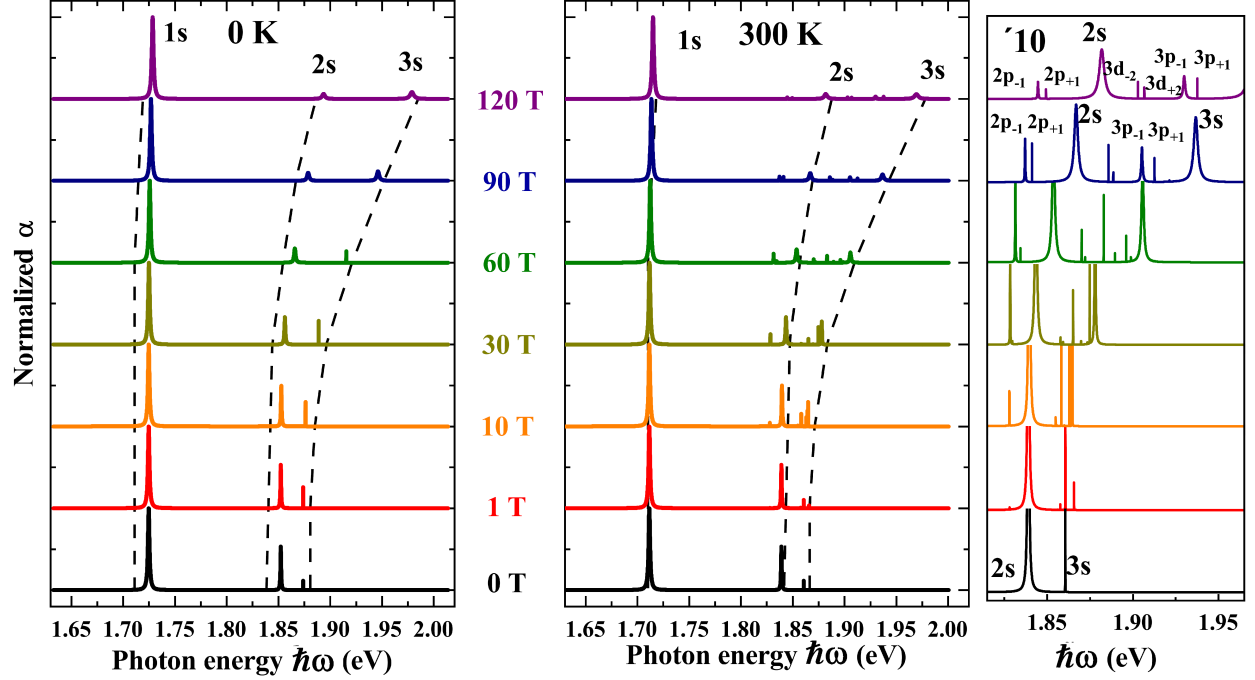


FIG. S-6. Normalized absorption spectra of neutral magnetoexciton at zero temperature (left) and room temperature (center) for various strength of magnetic field. The right panel is offset ($\times 10$ times) near $2s$ and $3s$ peaks of the center panel.

Our numerical results also highlight the emergence of the d -state peaks on the neutral magnetoexciton's absorption spectra. To explain this emergence, we need a higher-order correction beyond the quadratic thermo-induced motional Stark effect. Skipping the detailed calculations, we obtain the squared modulus of magnetoexciton wave function at zero separation for the d -state, which is proportional to the temperature square as

$$|\psi_{nd}^T(\mathbf{r}=0)|^2 \propto \left(\frac{k_B T}{M}\right)^2. \quad (\text{S-82})$$

Thus, the intensity of d -states peaks is much smaller than that of the p -states.

-
- [1] N.-T. D. Hoang, D.-N. Ly, and V.-H. Le, Comment on "Excitons, trions, and biexcitons in transition-metal dichalcogenides: Magnetic-field dependence", *Phys. Rev. B* **101**, 127401 (2020).
- [2] J. E. Avron, I. W. Herbst, and B. Simon, Separation of center of mass in homogeneous magnetic fields, *Annals of Physics* **114**, 431 (1978).
- [3] H. Ruder, G. Wunner, H. Herold, and F. Geyer, *Atoms in Strong Magnetic Fields* (Springer - Verlag, Berlin, 1994).
- [4] C. Poellmann, P. Steinleitner, U. Leierseder, P. Nagler, G. Plechinger, M. Porer, R. Bratschitsch, C. Schüller, T. Korn, and R. Huber, Resonant internal quantum transitions and femtosecond radiative decay of excitons in monolayer WSe₂, *Nature Materials* **14**, 889 (2015).
- [5] T. Yan, X. Qiao, P. Tan, and X. Zhang, Valley depolarization in monolayer WSe₂, *Scientific Reports* **5**, 15625 (2015).
- [6] Y. You, X.-X. Zhang, T. C. Berkelbach, M. S. Hybertsen, D. R. Reichman, and T. F. Heinz, Observation of biexcitons in monolayer WSe₂, *Nature Physics* **11**, 477 (2015).
- [7] P. Steinleitner, P. Merkl, P. Nagler, J. Mornhinweg, C. Schüller, T. Korn, A. Chernikov, and R. Huber, Direct observation of ultrafast exciton formation in a monolayer of WSe₂, *Nano Letters* **17**, 1455 (2017).
- [8] D. Farrelly, Motional stark effect on Rydberg states in crossed electric and magnetic fields, *Physics Letters A* **191**, 265 (1994).
- [9] F. Schweiner, P. Rommel, J. Main, and G. Wunner, Exciton-phonon interaction breaking all antiunitary symmetries in external magnetic fields, *Phys. Rev. B* **96**, 035207 (2017).
- [10] L. V. Hoang and N. T. Giang, The algebraic method for two-dimensional quantum atomic systems, *J. Phys. A: Math. Gen.* **26**, 1409 (1993).

- [11] A. P. Prudnikov, Y. A. Brychkov, and O. I. Marichev, *Integrals and Series*, Vol. 5: Inverse Laplace Transforms (Gordon and Breach Science Publishers, New York, 1992).
- [1] I. Feranchuk, A. Ivanov, V.-H. Le, and A. Ulyanenko, *Non-perturbative Description of Quantum Systems* (Springer, Switzerland, 2015).
- [13] D.-A. P. Nguyen, D.-N. Ly, D.-N. Le, N.-T. D. Hoang, and V.-H. Le, High-accuracy energy spectra of a two-dimensional exciton screened by reduced dimensionality with the presence of a constant magnetic field, [Physica E](#) **113**, 152 (2019).
- [14] Netlib.org. LAPACK: Linear Algebra PACKage, [Subroutine dsygvx.f](#).
- [15] N. S. Rytova, Screened potential of a point charge in a thin film, *Mosc. Univ. Phys. Bull.* **22**, 30 (1967).
- [16] L. V. Keldysh, Coulomb interaction in thin semiconductor and semimetal films, [JETP Lett.](#) **29**, 658 (1979).
- [17] E. Hanamura, N. Nagaosa, M. Kumagai, and T. Takagahara, Quantum wells with enhanced exciton effects and optical non-linearity, [Mater. Sci. Eng. B](#) **1**, 255 (1988).
- [18] P. Cudazzo, I. V. Tokatly, and A. Rubio, Dielectric screening in two-dimensional insulators: Implications for excitonic and impurity states in graphene, [Phys. Rev. B](#) **84**, 085406 (2011).
- [19] T. C. Berkelbach, M. S. Hybertsen, and D. R. Reichman, Theory of neutral and charged excitons in monolayer transition metal dichalcogenides, [Phys. Rev. B](#) **88**, 045318 (2013).
- [20] A. Chernikov, T. C. Berkelbach, H. M. Hill, A. Rigosi, Y. Li, O. B. Aslan, D. R. Reichman, M. S. Hybertsen, and T. F. Heinz, Exciton binding energy and nonhydrogenic Rydberg series in monolayer WS₂, [Phys. Rev. Lett.](#) **113**, 076802 (2014).
- [21] K. Tanaka, M. Kobashi, T. Shichiri, T. Yamabe, D. M. Silver, and H. J. Silverstone, LoSurdo-Stark effect for a hydrogenic impurity in a thin layer: Two-dimensional model, [Phys. Rev. B](#) **35**, 2513 (1987).
- [22] J. C. G. Henriques, H. C. Kamban, T. G. Pedersen, and N. M. R. Peres, Analytical quantitative semiclassical approach to the LoSurdo–Stark effect and ionization in two-dimensional excitons, [Phys. Rev. B](#) **102**, 035402 (2020).